ABSTRACT

AMBEKAR, ROHIT VINAY. Investigation of the Abilities of 3D Scanning Technology for Quality Inspection of Additively Manufactured Metal Parts. (Under the directions of Dr. Ola Harrysson and Dr. Richard Wysk).

This thesis examines methods used to produce metal AM parts, because metal AM has certain limitations in terms of build size, material, surface finish, and geometric accuracy. Two of the major challenges recognized for the metal AM processes are the surface finish and the geometrical accuracy of the parts produced. Because metal AM alone cannot produce functionally ready parts, especially for applications where geometric tolerances are of a greater concern; the parts are often built with overgrown surfaces and are machined in order to meet the design specifications.

It is important to accurately measure additively manufactured raw parts before they are machined. Conventional tools, like CMM which are industry standards for quality inspection, have certain deficiencies in measuring AM parts accurately, which is primarily due the rough part surfaces. Hence, the vision based 3D data acquisition systems like Computed Tomography (CT) scanners and 3D laser scanners which can better capture the details on AM parts could be used to replace the conventional inspection tools.

There have been efforts to develop the CT technology for metrological applications. Some researchers are also using CT as the primary inspection technique for inspecting AM parts. Although CT scanners are accurate, they are not flexible and mobile. On the other hand, the 3D laser scanners are flexible, mobile, and reasonably accurate. Hence, 3D scanners are being integrated with AM systems to measure parts prior to CNC operations. In these systems, the user inputs a CAD model and the system outputs a functionally ready part. Though, the 3D

scanners are accurate while inspecting machined metal parts, it is important to investigate their performance for inspection of AM parts.

In this work, the abilities and/or limitations of a commercially available 3D scanner are investigated. This work focuses on developing approaches to utilize the 3D scanners to extract critical geometric information pertaining to the parts. Further, a comparative analysis was done to compare the results obtained using the 3D scanner with the traditional metrology tools. The thesis shows that the 3D scanner can capture the surface variations and the defects in AM parts effectively.

Investigation of the Abilities of 3D Scanning Technology for Quality Inspection of Additively Manufactured Metal Parts

by
Rohit Vinay Ambekar

A thesis submitted to the Graduate Faculty of
North Carolina State University
in partial fulfillment of the
requirements for the degree of
Master of Science

Industrial Engineering

Raleigh, North Carolina

2016

APPROVED BY:

_____	_____
Dr. Ola Harrysson	Dr. Richard Wysk
Committee Co-Chair	Committee Co-Chair

_____
Dr. Binil Starly

DEDICATION

To my grandparents, teachers and friends.

BIOGRAPHY

Rohit Ambekar was born to Mr. Vinay Ambekar and Mrs. Shubhada Ambekar in December 1992 in the city of Pune in western India, the *Oxford of the East*, as it is known, mainly due the presence numerous prominent academic institutions of modern and British era. He received his Bachelor's degree in Mechanical Engineering from the University of Pune in May 2014. Having felt the need to discover and learn deeper about manufacturing in his junior year, he decided to pursue a graduate degree. In August 2014, he enrolled for Master's program in Edward P. Fitts Department of Industrial and System Engineering at the North Carolina State University. He started working as a Graduate Research Assistant at the Center for Additive Manufacturing and Logistics (CAMAL) from January 2015.

ACKNOWLEDGMENTS

I would first like to thank my advisors Dr. Ola Harrysson and Dr. Richard Wysk for their constant guidance, encouragement and support. This work would not have been materialized without their valuable insights and suggestions. I would also like to thank Dr. Binil Starly for agreeing to be on the committee and helping me understand the fundamentals of 3D scanning.

I would like to thank my colleagues Harshad Srinivasan and Carter Keough for helping me learn the approach one should have towards work. I am grateful to Harshad for introducing me to 3D scanning and always being proactive to answer my queries. I would like to thank Austin Isaacs for his help in additively manufacturing the test parts. Special thanks to Dr. Harvey West for providing a great work environment and timely help. I would like to thank Mr. Steve Walker for cooperating throughout this work. I feel fortunate to have met countless hard working, efficient and inspirational personalities during my time at CAMAL. I am also thankful to all the professors who shared their experience and knowledge that helped me lay a strong academic foundation.

I remain indebted to my parents as well as other family members for always believing in me and supporting my decisions. Many thanks to Parul and Rutuja for their timely help and constant support. I would like to thank my friends Surabhi, Saloni, Pratiksha, Payal, Priyank, Kshitij, Omkar, Chaitanya, Sourabh, Anish, Salil, Swati, Mihir, Pranit for making my experience at NCSU a memorable one. Lastly, I would like to thank Rashmi for being with me in all the good and bad times and for always making me believe in myself.

TABLE OF CONTENTS

LIST OF TABLES ..... **VII**

LIST OF FIGURES ..... **VIII**

CHAPTER 1: INTRODUCTION **1**

1.2 Introduction to Additive Manufacturing **1**

1.2 Metrology of Additive Manufactured Parts **2**

1.3 Research Motivation **6**

1.4 Objectives **8**

1.5 Chapter Summary **9**

CHAPTER 2: LITERATURE REVIEW **10**

2.1 Additive Manufacturing **10**
2.1.1 Classification of Additive Manufacturing Processes 10
2.1.2 Metal Additive Processes 12
2.1.2.1 Indirect Metal AM Processes 12
2.1.2.2 Direct Metal AM Processes 14

2.2 Applications and Limitations of Additive Manufacturing **18**

2.3 Data Acquisition Systems in Metrology **21**
2.3.1 Classification of Data Acquisition Methods in Metrology 23
2.3.1.1 Active Systems 24
2.3.1.2 Passive Systems 26
2.3.2 Development of 3D Scanners 28
2.3.2.1 Development of 3D Scanners for Surface Roughness Measurement 28
2.3.2.2 Vision-Based 3D Data Acquisition Systems for Geometric Inspection 30

2.4 Chapter Summary **32**

CHAPTER 3: METHODOLOGY **33**

3.1 Investigation of the Ability of a 3D Scanner to Measure Average Surface Roughness **33**

3.1.1 Average Surface Roughness (Ra) 33
3.1.2 Determination of Average Surface Roughness using a 3D scanner 36

3.2 Characterization of Additively Manufactured Metal Parts 38
3.2.1 Test Parts 38
3.2.2 FARO Edge 3D Scanner 39
3.2.3 Point-Model Generation 40

3.3 GD&T Analysis 43

3.4 Chapter Summary 48

CHAPTER 4: RESULTS AND DISCUSSION 49

4.1 Surface Roughness Measurement 49

4.2 GD & T Analysis 53
4.2.1 Visual Inspection 54
4.2.2 Dimensional Measurements 57
4.2.2.1 Linear Dimensions 58
4.2.2.2 Angular Measurements 59
4.2.2.3 Radial Dimensions 60
4.2.3 Tolerances 61

4.3 Chapter Summary 65

CHAPTER 5: CONCLUSION AND FUTURE WORK 66

5.1 Conclusion 66

5.2 Future Work 67

REFERENCES 69

APPENDICES 75

Appendix 1: Other Active Systems 76

Appendix 2: Surface Roughness MATLAB code 77

Appendix 3: Result Tables 78

LIST OF TABLES

Table 1: Geometric Characteristics and Symbols [5] 3
Table 2: Various Data Acquisition Systems Used in Industry 27
Table 3: Measured Dimensions and Tolerances 46
Table 4: Measured Surface Roughness on the Profilometer Calibration Plate 49
Table 5: Measured Surface Roughness on the Surface Roughness Comparator 50
Table 6: Measured Surface Roughness on the EBM Part 51
Table 7: Measured Surface Roughness on the EBM Test Parts 53
Table 8: Percentage Shrinkage 59

LIST OF FIGURES

Figure 1: Flatness Tolerance 4
Figure 2: Cylindricity Tolerance 5
Figure 3: Microscopic (250x) image of an AM surface acquired using Hirox Digital microscope 7
Figure 4: Illustration of a touch probe measuring an additively manufactured surface 7
Figure 5: Metal AM processes 12
Figure 6: Illustration of the Binder Jetting Process 15
Figure 7: Illustration of the LENS Process 15
Figure 8: Illustration of the EBAM Process 16
Figure 9: Illustration of the EBM Process- taken from [22] 17
Figure 10: Illustration of the SLM Process 18
Figure 11: Classification of Data Acquisition Systems- reproduced based on [36] 24
Figure 12: Slit Scanner 25
Figure 13: Single-Point Scanner 26
Figure 14: Surface Roughness Comparator 29
Figure 15: Surface Profile Example 34
Figure 16: Surface Comparator 35
Figure 17: Surface Roughness Measurement with Profilometer 35
Figure 18: Masked Part Surface (a) and Scan of the Part Surface (b) 36
Figure 19: Methodology: Surface Roughness Determination 37
Figure 20: Point Cloud (a) and Fit Plane (b) 38
Figure 21: Test Parts 38
Figure 22: FARO Edge Scanner 39
Figure 23: Part Orientations used while scanning 40
Figure 24: Raw Scans 41
Figure 25: Combined Point-Model 42
Figure 26: Methodology- GD & T Analysis 43
Figure 27: Unaligned point-model and CAD model in the same space 43
Figure 28: Aligned CAD and points models 44
Figure 29: Defined Features 45
Figure 30: Part Orientations and Fixturing during CMM Measurements 47
Figure 31: Profilometer Calibration Plate 49
Figure 32: Surface Roughness Comparator 50
Figure 33: EBM Part Surface 51
Figure 34: EBM Test Parts- surfaces used for roughness measurement 52
Figure 35: Defects-extended edges 54
Figure 36: Defects: Bottom Surfaces 55
Figure 37: Defects: Cylinder Distortion 56
Figure 38: Defect: Cylinder Distortion 56
Figure 39: 3D Dimensioning in Geomagic Qualify 57
Figure 40: Linear Dimensions 58

Figure 41: Angular Dimensions 59
Figure 42: Diameters 60
Figure 43: Geomagic Qualify GD & T Analysis 61
Figure 44: Flatness- Part 2 62
Figure 45: Flatness Tolerances 63
Figure 46: Cylindricity- Part 2 64
Figure 47: Cylindricity Tolerances 64

CHAPTER 1

INTRODUCTION

The purpose of this chapter is to provide the reader with a general overview of the metrology of parts produced by additive manufacturing processes. This chapter begins with a brief introduction to Additive Manufacturing (AM) technology, its advantages, and limitations. The primary challenges associated with AM are briefly explained. This discussion is followed by a brief overview of Geometric Dimensioning and Tolerancing (GD & T) standards in metrology and the specific parameters measured in this study. The discussion then moves on to the motivation behind undertaking this research. Finally, specific objectives of this work are discussed and the structure of this thesis is outlined.

1.2 Introduction to Additive Manufacturing

For more than two decades, additive manufacturing has given the world a new vision for developing products faster and at a lower cost. Additive manufacturing processes, instead of removing material as opposed to traditional subtractive manufacturing processes such as machining, fabricate a part in an additive manner layer-by-layer. Various AM processes have strengths and weaknesses compared to each other because of the different materials and different build principles used in these processes.

AM can be used with a wide range of materials including elastomers, biomaterials, alloys ranging from Aluminum to superalloys such as Inconel [1]. Many of the above mentioned materials are in fact difficult to process through conventional manufacturing methods. AM can also be used to manufacture complex geometries which often seem

unachievable by traditional manufacturing methods. This eliminates the use of stock materials (bar, plate or castings) as well as fixtures and tooling usually required in traditional manufacturing while expanding the set of manufacturing geometries that can be made to near net shape.

Apart from the above mentioned obvious advantages of AM, it has certain limitations in the areas of surface finish and geometric accuracy. For AM to be accepted as a primary manufacturing process, the parts produced by AM have to consistently satisfy the geometric tolerances. Layer-by-layer formation of the part results in stair-stepping effect and affects the surface finish in AM. In applications such as biomedical implants, sometimes, rough surfaces are favorable as it allows for accelerated bone ingrowth [2]. However, in mechanical applications, surface finish and geometric accuracy are often of greater concern.

1.2 Metrology of Additive Manufactured Parts

The American National Standards Institute (ANSI), in 1973, introduced a system called Geometric Dimensioning and Tolerancing (GD & T). Since then, this system is being used as a standard across the industry for communicating, interpreting or manufacturing products via engineering drawings and/or CAD models. This standard was initially referred to as ANSI Y14.5-1973. In 1994, the standard was enhanced with formal mathematical definitions of GD & T and was termed as ASME Y14.5-1994 [3]. In 2009, the standard was again revised for 21^{st} –century applications and became ASME Y14.5-2009.

According to this standard, there are only four parameters that the geometry can control: form, size, angle, and location. Further, there are three types of geometric characteristic controls namely surface controls, axis controls, and centerplane controls. These

controls are covered by fourteen geometric characteristics and are classified in five categories as follows [4]:

Table 1: Geometric Characteristics and Symbols [5]

Category	Geometric Characteristic	Symbol
Form	Flatness	
	Straightness	
	Circularity	
	Cylindricity	
Profile	Surface Profile	
	Line Profile	
Orientation	Parallelism	
	Perpendicularity	
	Angularity	
Runout	Total Runout	
	Circular Runout	
Location	Position	
	Concentricity	
	Symmetry	

Theoretical features that are assumed to be exact are known as datum. Out of the geometric characteristics listed in the above table, the form tolerances do not need any datum reference as they are applicable to single features or elements of single features. They are often used to tolerance the shape of datum features [4]. Flatness and Cylindricity are the two most common geometric characteristics used on datum features.

In this study, the basic dimensions including linear dimensions, angular dimensions, and radial dimensions (diameters) were measured. Apart from the basic dimensions, the tolerances of flatness and cylindricity were also measured. These tolerances are defined in ASME Y14.5-2009 as follows [5]:

- **Flatness**

  Flatness is the condition of a surface having all elements in one plane. A flatness tolerance specifies a tolerance zone defined by two parallel planes within which the surface must lie [5]. An illustration of how the flatness tolerance is specified on a drawing and what it means is provided in Figure 1.

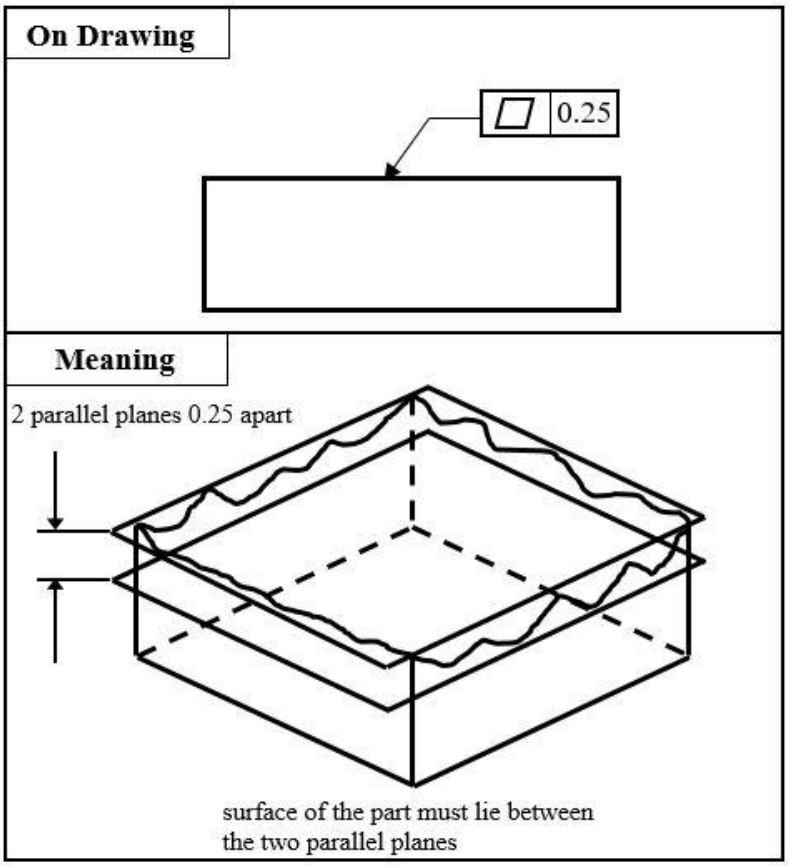

Figure 1: Flatness Tolerance

- **Cylindricity**

  Cylindricity is a condition of a surface of revolution in which all points of the surface are equidistant from a common axis. A cylindricity tolerance specifies a tolerance zone bounded by two concentric cylinders within which the surface must lie [5]. An illustration of how the cylindricity tolerance is specified on a drawing and what it means is provided in Figure 2.

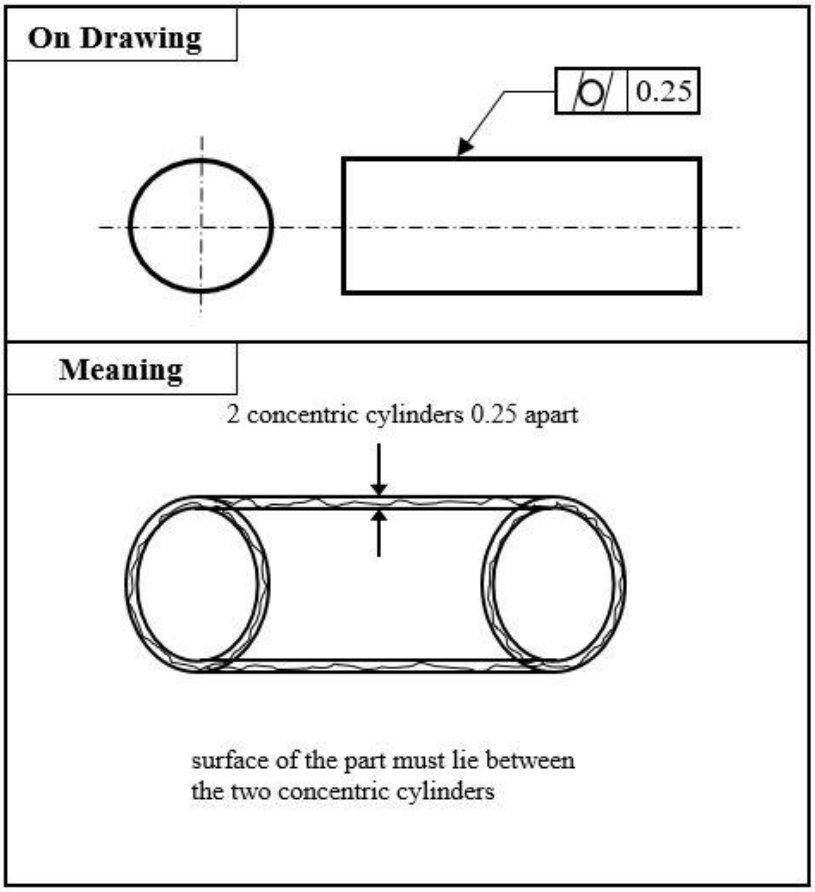

Figure 2: Cylindricity Tolerance

1.3 Research Motivation

Tolerances are usually specified in the design stage of the end product. In the case of additive manufacturing, these design specifications are often met by finish-machining the near-net-shape AM parts. This is usually done by mounting them in a CNC machine to remove excess material in order to achieve the required geometric accuracy and surface finish. Near-net-shape parts are manufactured with overgrown surfaces to make sure there is enough excess material for achieving various critical tolerances after machining.

Increasing demand and complexity of AM parts calls for proper measurement of internal and external AM features. Hence, it is necessary to characterize and qualify the AM features with known accuracy. However, the complex geometries often produced using AM restrict the use of conventional inspection instruments like touch probes. Although touch probes are the most widely used and accurate inspection systems, vision based systems are preferred because they are faster when used to inspect free-form surfaces.

Moreover, the surface texture usually present on the additively manufactured parts is of a non-uniform nature as shown in Figure 3. The geometry of the touch probe has a major impact on the measured surface. A large radius probe can act as a low-pass filter, not detecting high-frequency valleys. Figure 4 shows an illustration of how a touch probe reads the surface profile on an additively manufactured surface. As can be seen from Figure 4, the width of the surface under observation is approximately 828 µm. On careful observation, it can also be seen that the spacing between any two peaks (or valleys) could be less than 100 µm. Moreover, this spacing is not uniform across the length of the surface. Hence, any touch probe having a diameter more than or equal to the peak spacing will fail to capture the valleys that might be

present in between the two peaks making the probing systems unsuitable for metrology of additively manufactured parts.

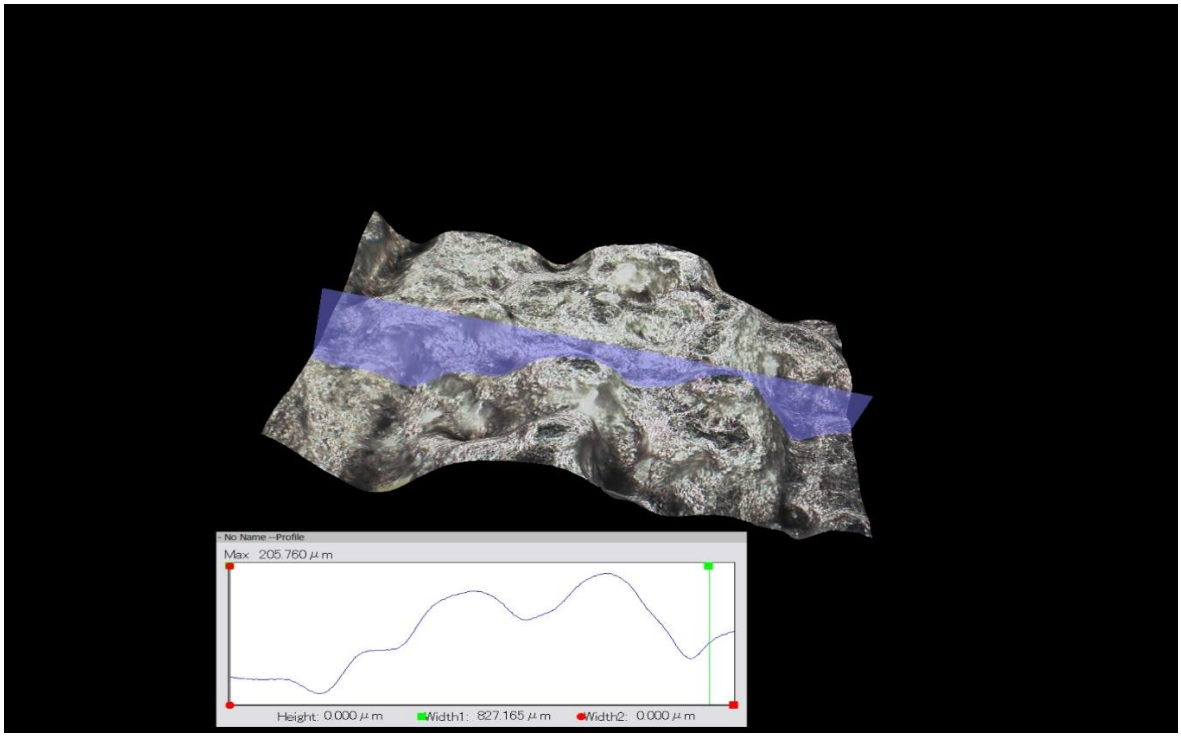

Figure 3: Microscopic (250x) image of an AM surface acquired using Hirox Digital microscope

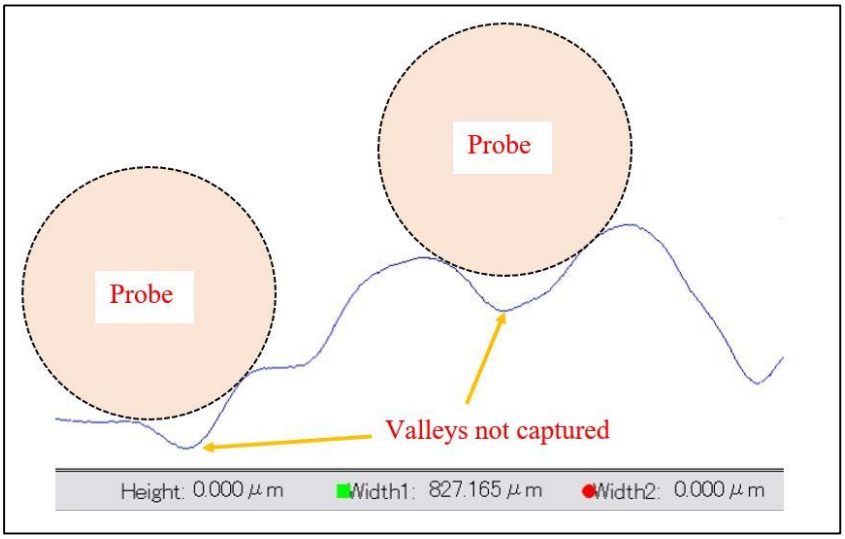

Figure 4: Illustration of a touch probe measuring an additively manufactured surface

Technological innovation in computing technology and optoelectronics has contributed significantly to the development of vision based 3D data acquisition systems like industrial Computed Tomography and 3D Laser Scanning. These systems have become increasingly popular in recent years. Although CT has been used in metrology of AM parts, there has been very little work done to validate the 3D laser scanning for use in metrology of AM parts. Flexibility, mobility, and accuracy of the 3D scanners make them potentially suitable for integration with any of the available AM processes. Thus there is a need to investigate the performance of the existing vision based systems as well as to develop a robust inspection system for AM.

1.4 Objectives

The major objective of this work is to investigate the abilities and/or limitations of a commercially available 3D laser scanner for geometrical inspection of additively manufactured parts. In pursuit of this objective, three test pieces were additively manufactured. This study is focused on analyzing only planar and cylindrical features produced using additive manufacturing. This is because planes and cylinders are considered as the most tightly toleranced features and are used to define many functional component assemblies like bearings. As a part of this study, following parameters were measured using the 3D scanner:

1) Average Surface Roughness
2) Linear Dimensions
3) Angular Dimensions
4) Radial Dimensions
5) Tolerances- Flatness, Cylindricity

Certain methodologies were devised to extract the above mentioned parameters from the scanner output. These measurements were compared to the values obtained using conventional measurement equipment for the same parameters. Further, the test pieces were compared with their design specifications to investigate the deviation.

1.5 Chapter Summary

In this chapter, a brief introduction to additive manufacturing, its advantages, limitations, and associated challenges was presented. The standards used in GD & T were discussed. The motivation behind exploring the abilities of a 3D scanner was presented and specific objectives pertaining to this work were established.

The remainder of this thesis is structured as follows: Chapter 2 presents information about the work that has been previously done in this research area. Chapter 3 illustrates the procedures that were followed to pursue the identified research objective. The results obtained from this study are presented in Chapter 4. The thesis concludes with a summary of this research and directions for future work in Chapter 5.

CHAPTER 2

LITERATURE REVIEW

Since the focus of this work is on the metrology of additively manufactured mechanical parts, the literature review will first begin with a brief overview of the basic methods used in additive manufacturing. This discussion is followed by a review of GD & T methods used for qualifying mechanical parts, and then moves on to vision based methods and systems that are used to measure and qualify components.

2.1 Additive Manufacturing

Additive Manufacturing is layer-based formation of a part from a 3D CAD model. The principle of additive manufacturing is fabricating a part layer-by-layer through a bottom-to-top approach by depositing or combining materials. The CAD file of the required part is first sliced across each layer along the direction of fabrication [1]. This processed file is then sent to the machine where the part gets manufactured layer-by-layer. The manufactured part is then removed from the machine and necessary post-processing operations are carried out in order to remove the unwanted material. American Society for Testing and Materials (now ASTM International) classifies various available AM processes as explained in the next section [6].

2.1.1 Classification of Additive Manufacturing Processes

Additive manufacturing processes can be classified into categories as explained below. These categories are as per ASTM International, ASTM F2792-12a.

- **Binder Jetting:** “An additive manufacturing process in which a liquid bonding agent is selectively deposited to join powdered materials [6].” Various materials including ceramics, metals, sand, and plastics are often used in these processes.
- **Directed Energy Deposition:** “An additive manufacturing process in which focused thermal energy is used to fuse materials by melting as they are being deposited [6].” Common energy sources used in these processes include laser and electron beam. Direct Energy Deposition is often used in processes where powder based materials are used.
- **Material Extrusion:** “An additive manufacturing process in which material is selectively dispensed through a nozzle or orifice [6].” These processes are commonly used for prototyping using polymers.
- **Material Jetting:** “An additive manufacturing process in which droplets of build material are selectively deposited [6].” Photopolymers and wax are the most common materials used in these processes.
- **Powder Bed Fusion:** “An additive manufacturing process in which thermal energy selectively fuses regions of a powder bed [6].” These processes are able to be used with a wide range of materials including ceramics, metals, composite materials, and thermoplastics.
- **Sheet Lamination:** “An additive manufacturing process in which sheets of material are bonded to form an object [6].” Metal, polymer, or paper sheets are often used in these processes.

- **Vat Polymerization:** "An additive manufacturing process in which liquid photopolymer in a vat is selectively cured by light-activated polymerization [6]." These processes are limited to be used with photo-curable polymers.

2.1.2 Metal Additive Processes

This section focuses on metal AM processes from the categories mentioned in the previous section. The metal AM processes can be broadly classified as per the tree shown in Figure 5.

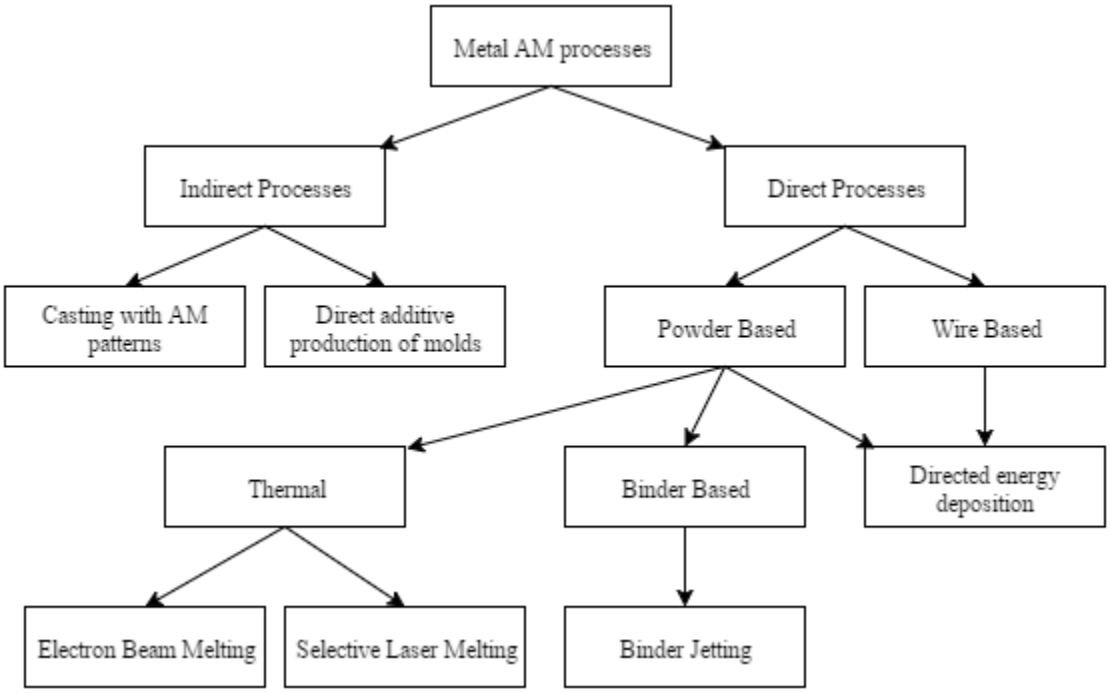

Figure 5: Metal AM processes

2.1.2.1 Indirect Metal AM Processes

Indirect AM processes are often grouped under the name of 'Rapid Tooling'. The term Rapid Tooling refers to additive manufacturing of parts that are neither prototypes nor are functional parts. Indirect AM processes are usually of two types:

1. Additive manufacturing of patterns for investment and vacuum casting
2. Direct additive production of molds for casting

The rapid tooling processes are further classified as soft or hard tooling [7]. Soft tooling involves production of molds (or patterns) which are destroyed after a single cast or a small batch of parts. On the other hand, hard tooling involves production of molds from metal, ceramics, or composites which are generally used for high volume production.

Additive manufacturing of patterns for investment casting has long been done with the help of almost all the available AM processes. Acrylonitrile Butadiene Styrene (ABS) and specifically designed thermoplastics having low thermal expansion and cleaner burn-out are often used to additively manufacture patterns for investment casting in Fused Deposition Modeling (FDM) [8]. Thermoplastics and starch are often used in Binder Jetting processes to manufacture the patterns [9]. The resins like CastPro resin designed by 3D systems [10] are specifically designed to be used in Vat Polymerization processes for producing patterns for investment casting. Ceramic molds have also been produced with a photopolymerization process [11]. Wax is often used in Material Jetting Processes to produce the patterns. Powder Bed Fusion processes are also used for making patterns where specific materials like CastForm by 3D systems for their Selective Laser Sintering (SLS) systems and Primecast by EOS are used [12], [13]. Zcorp (acquired by 3D systems) machines often use starch and plastics for additively manufacturing investment casting patterns [9].

Direct Production of molds is predominantly done with the help of Powder Bed Fusion and Binder Jetting Processes. These processes often include production of mold inserts for series injection molds, die casting molds, and prototype tools for injection and die moldings

[7]. These molds are generally produced from alloys such as tool steels or ceramics such as silica or alumina for high volume production and strength. Usually, AM processes like Electron Beam Melting and Selective Laser Melting are used as they possess the capability to process such materials [7]. Molds of sand and plaster can be produced using such powder bed fusion processes. Powder bed processes help in reducing lead time while allowing flexibility in metals and alloys to be used for casting. EOS offers EOS DirectCast, a material which can be used to produce sand casting molds directly by selective laser sintering. ExOne and Voxeljet use Binder Jetting processes to produce large molds and cores for sand casting [14], [15].

2.1.2.2 Direct Metal AM Processes

- **Binder Jetting Processes:** Binder jetting process as shown in Figure 6 is often used for AM of metals. As established by Ex-One, in these processes, metallic powder is bonded with the help of resin [16]. This resin then often undergoes a curing process and produces a 60% dense green part. The curing process is followed by a high temperature sintering process. During the sintering process, the green part is sometimes impregnated with bronze which results into a composite metal part with approximately 100% density [17]. Ex-One has recently developed machines that are capable of producing 99% dense parts with Inconel alloy which do not require any further processing [18]. The binder jetting processes are advantageous in many ways as they eliminate the need for any supports and post-processing that may be required to remove the supports.

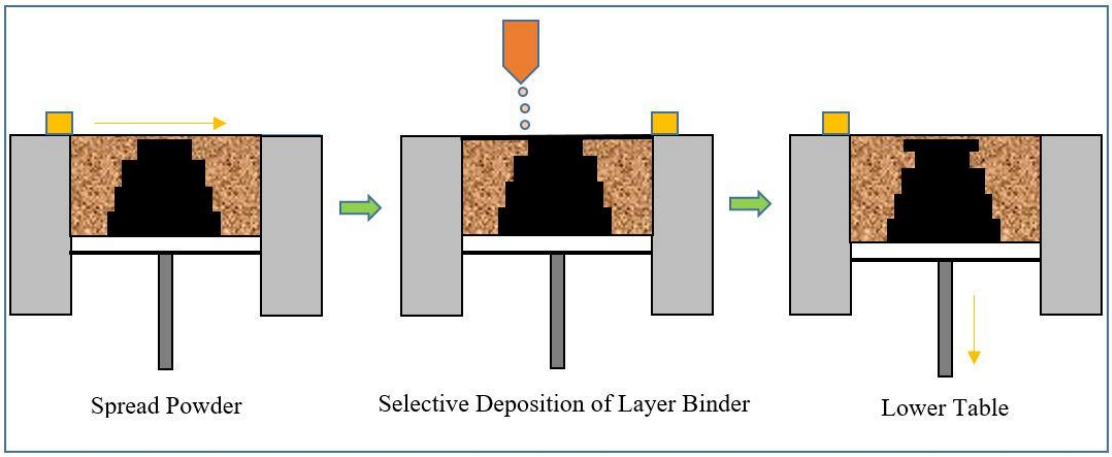

Figure 6: Illustration of the Binder Jetting Process

These processes are chemical processes as opposed to thermal processes and hence the parts produced do not have any internal stresses. The failure rates in these processes are high for parts with complex geometries as the green part produced in these processes is fragile and needs special attention during handling and cleaning.

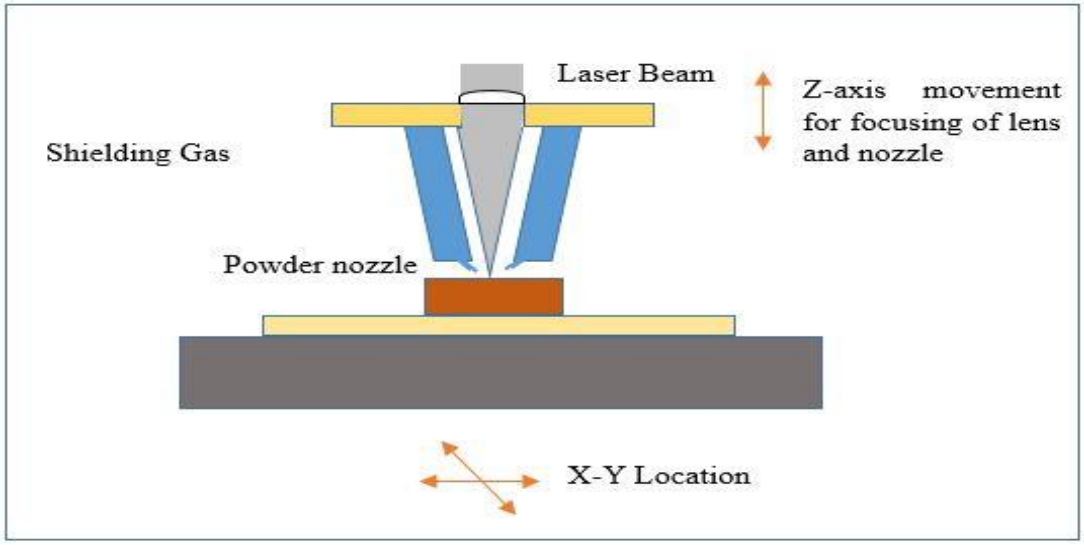

Figure 7: Illustration of the LENS Process

- **Directed Energy Deposition:** These processes produce parts by fusing material to previously produced layers by means of applied energy. The material may be supplied by either a wire or as a powder. Energy source used in these processes can be a laser, electron beam, or plasma arc. Direct energy deposition systems by Optomec [19], LENS (Laser Engineered Net Shaping), use laser as the energy source. In the LENS process as shown in Figure 7, the build plate and/or laser-powder supply are often mounted on a 5-axis platform in order to create parts with overhanging edges without creating supports [20].

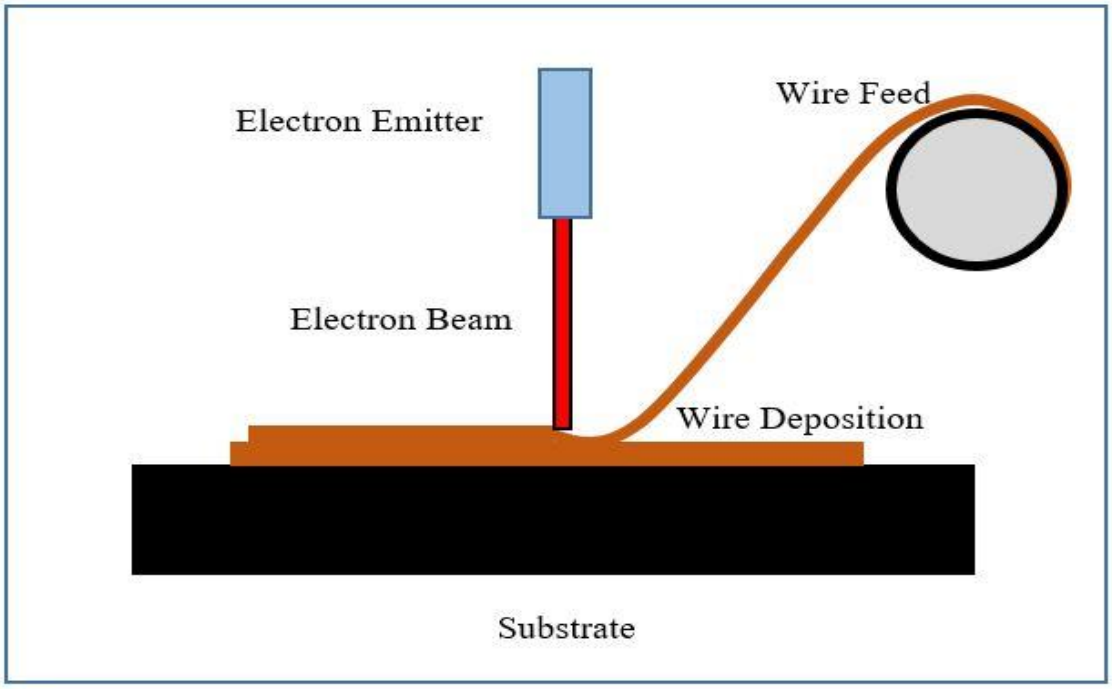

Figure 8: Illustration of the EBAM Process

On the other hand, Electron Beam Additive Manufacturing (EBAM) formerly known as Electron Beam Free-form Fabrication (EBF^3) systems as shown in Figure 8, use

electron beam as the energy source and the material is supplied through a wire feeding mechanism [21].

- **Powder Bed Fusion:** In these processes, an energy source selectively scans and melts a layer of metal powder spread on the build substrate. Powder Bed Fusion processes are flexible in terms of process parameters and the support structures can be easily generated for complex geometries with lesser process planning.

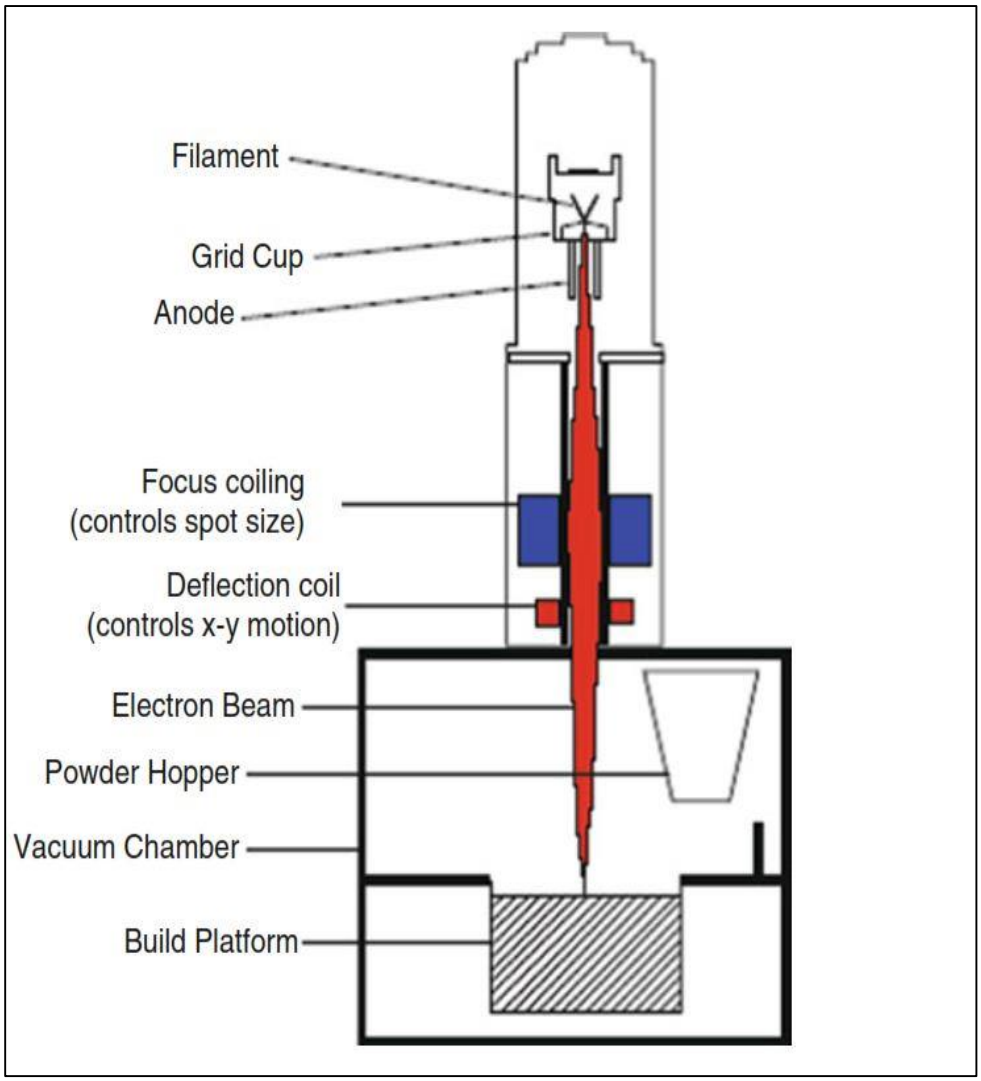

Figure 9: Illustration of the EBM Process- taken from [22]

EBM as shown in Figure 9 [22] is a hot-bed AM process since the build volume is maintained at an elevated temperature during the build process. EBM functions in vacuum as opposed to inert atmosphere and the accelerated electron beam completely melts the powder particles. On the other hand, SLM as shown in Figure 10, is a process where the energy source is a laser beam and the powdered metal is spread on the build plate.

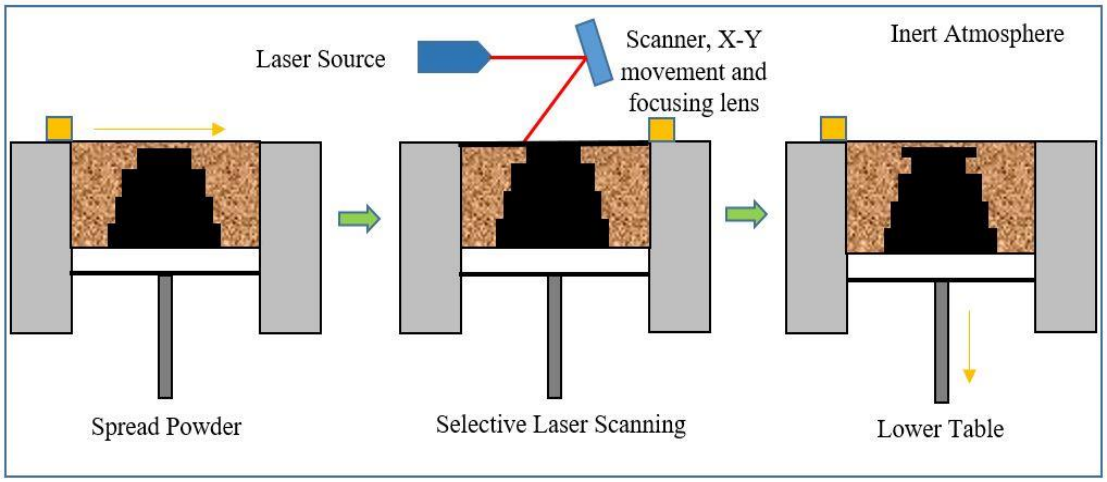

Figure 10: Illustration of the SLM Process

In SLM, the vacuum in EBM is replaced either by purified Argon or by nitrogen to create an inert atmosphere. This inert atmosphere provides oxidation protection, efficient heat conduction and component cooling [23]. In these laser based, cold powder bed AM processes, the powder is fully melted [1].

2.2 Applications and Limitations of Additive Manufacturing

Many industries including aerospace, military, automotive, dental, medical etc. have started making use of AM. The primary purpose of using AM is to be able to fabricate complex

parts out of hard-to-machine materials. AM produces near-net-shape parts eliminating the need of rough machining operations. As discussed in Section 2.1.2.1, the tooling industry utilizes AM to produce functional tool components. Remarkable development is seen in additively manufacturing plastic injection molding and die casting tooling and rapid tooling is considered as one of the most prominent subcategories of AM.

In the medical industry, AM is primarily used for medical device manufacturing of custom surgical instruments and prosthetic implants. These implants are patient specific and need to be flexible and should fit accurately. Sometimes, the weight of these implants needs to be kept as low as possible and they still must satisfy the structural and mechanical requirements. Hence, porous metallic structures, which are producible with the help of additive manufacturing, are sometimes desired. In the automotive industry, Cooper et al. at Red Bull Technology, additively manufactured thin walled hydraulic manifolds by DMLS. This experiment not only helped them to reduce the weight of the manifold but also improved the fluid flow significantly [24]. Ventola et al. investigated the possibility of using DMLS for producing artificial roughness, optimized for convective heat transfer enhancement, in manufacture of flat and finned heat sinks for electronics cooling. They found a peak convective heat transfer increase of 63% on average for rough flat surfaces and 35% for rough finned surfaces [25].

As it can be seen from the above examples, AM is being increasingly accepted across a diverse range of industry groups, despite being in its infancy. However, in spite of having extensive advantages when compared to the traditional manufacturing processes, AM processes still show several deficiencies. Hence, it is necessary to have a robust inspection

system which can capture all such errors effectively and accurately and this work proposes a methodology to use a vision based system for inspection of additively manufactured parts. Several studies on dimensional accuracy have shown that it is possible to get tolerances of ±0.25 mm [26] on metal tooling produced by AM. The parts produced from the tooling in these studies were found to have 90% of their dimensions within ±0.25 mm [27]. This accuracy is superior to what is typically achieved in sand casting, but it is inferior to that of subtractive machining. For many applications like conceptual modelling, design aids, anatomical modeling, the accuracy is of lesser importance. However, for some applications like the ones in automotive and aerospace industries, accuracy is of prime importance. Due to concentrated energy input in processes like SLM, the temperature gradient mechanism and the plastification lead to residual stresses and part deformations affecting dimensions, geometry as well as the mechanical strength of the parts. Residual stresses further contribute to crack formation or disconnection of the parts from the base plate during the process [28]. In binder jetting processes, the parts are subjected to warping and shrinkage during the sintering process in the furnace [1]. In directed energy deposition (EBAM), finer features are difficult to achieve as the layer thickness is relatively large and certain issues like bundling of material at corners and overflow of material along edges can be observed [1]. It can be inferred from the above examples that different types of errors are still present in various additive manufacturing processes. Hence, we classify the errors that may be induced during an AM process chain as follows[29]:

- **Preprocessing Errors:** These errors are constituted during the conversion of 3D CAD file into the STL file format.

- **Machine Errors:** These errors can be measured and compensated for. Their effect on the overall system can be controlled reasonably.
- **Material Processing Errors:** These are the most complicated errors in AM. These dimensional errors arising due to shrinkage vary with different geometric shapes.
- **Random Errors:** These errors are termed as noise and cannot be correlated to a particular source of error from the types mentioned above.

All of the above mentioned errors affect the accuracy and repeatability in additive manufacturing. In addition to the above errors, factors like the material being used, size of the part, build orientation, and wall thickness also influence the accuracy [30]. It can be noticed that metal AM parts need considerable post-processing to conform to the design specifications in terms of tolerances and surface finish. The ability to quickly, additively manufacturing a part and evaluating it for form, fit, and function can significantly reduce the manufacturing lead time [31]. Hence, it is necessary to improve the current AM processes as well as to develop an in-process inspection system. The various methods of data acquisition in metrology have been explored in the following sections.

2.3 Data Acquisition Systems in Metrology

In today's highly competitive and uncertain manufacturing environment, a manufacturing system has to be flexible. Such a system should be adaptive to the dynamic environment in every aspect of new product development. The critical task of building such a robust system needs a solid understanding of the changes and uncertainties that may occur during the manufacturing process. The vision-based 3D data gathering systems are becoming increasingly popular to capture such changes and uncertainties in the geometric shape, features,

and surface finish of the part. This increasing popularity is mainly because of their ability to capture not only the information on dimensions but also the information on product geometry, surface finish, and surface defects [32]. Vision-based systems have come up as one of the most sought after technologies in metrology because of the technological advancement in optoelectronics and availability of increased computing technology.

Inspection in manufacturing should be accurate, automated, fast, and ideally integrated into the production line. Industrial advancement demands for non-contact, real-time, cost efficient, and compact measurement systems. However, most of the today's state of the art inspection systems do not serve all of these needs and are established for regular shaped parts. Traditionally used CMMs are adequate for the parts consisting of features like planes, cylinders, cones, and spheres only. Usually, a set of six points is enough to fit any of the above mentioned features. For free-form surfaces, it might not be the case. Such surfaces often need thousands of points for definition and the surfaces may be delicate and may require a non-contact type measurement [33]. Moreover, the size of the part to be measured may be restricted by the available surface area of the CMM table. Also, the CMM probe may not reach sharp edges, corners, pockets, and spikes and hence measurement of complex profiles can be difficult with a CMM [34]. Above discussed limitations of tactile measurement systems like CMM have led to the development of various vision-based 3D data acquisition systems which are fast, non-contact type, and store measured data immediately in the computer memory. Matache et al. recently compared 3D scanning with CMM for dimensional inspection of a small gas turbine and their results suggested that both methods are accurate enough although the CMM had a marginally better accuracy [35]. Though the CMMs have a slightly better accuracy,

vision-systems outperform CMMs in terms of speed of operation and variety of surfaces that can be scanned. Hence, vision systems turn out to be useful in reducing the manufacturing lead time especially in the field of additive manufacturing where there is a need of rapid inspection of thin walled, free-form, and complex part geometries. Therefore, we discuss various methods of data acquisition used in metrology in the following section.

2.3.1 Classification of Data Acquisition Methods in Metrology

A 3D data acquisition system collects 3D point coordinates of a given section of a surface. Different systems differ in their working principle and use different mechanisms to interact with the surface of the part under observation. Researchers around the globe have classified the data acquisition systems from several different perspectives. Várady et al. have classified these systems as shown in Figure 11 [36]. The systems are broadly classified into contact type and non-contact type. The contact type systems physically touch the part surface with a mechanical probe which is usually fit at the end of a robotic arm. On the other hand, the non-contact type systems use media like sound, light, or magnetic fields to interact with the surface. The data captured from both of these types require additional post-processing and analysis. The scope of this research is limited to non-contact type systems and hence non-contact systems are reviewed. Isgro et al. have further classified non-contact systems into active and passive systems [37]. Active systems project energy onto the part surface and detect its position to carry out measurements. Passive systems are those which work only on images produced by reflected light from a natural or artificial source.

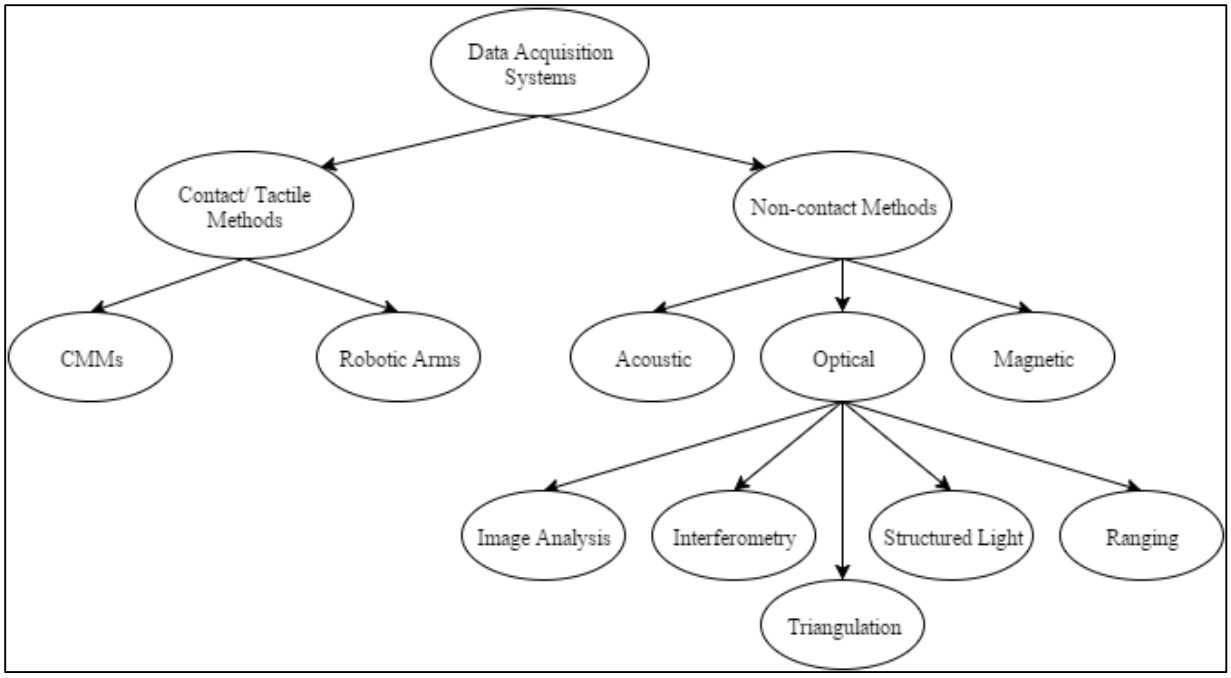

Figure 11: Classification of Data Acquisition Systems- reproduced based on [36]

2.3.1.1 Active Systems

Active systems are often classified according to their working principles: interferometry, time-of-flight or laser pulse, triangulation [38]. As the 3D laser scanner used in this work is based on the principle of triangulation [39], only triangulation from the active systems is explained in detail. The description of the other active systems can be found in Appendix 1.

- **Triangulation:** These scanners are based on the principle of triangulating a measurement spot on the part surface from a physically distinct camera optical source and detector [38]. The (x,y,z) coordinates of the illuminated spot on the part surface are calculated by simple geometry. As shown in Figures 12 and 13, the triangulation sensors can be either single point or slit. A slit scanner allows the projection of a laser

line and simultaneously detects complete profile of the points though it has to compromise between field of view and depth resolution. The slit scanners also have small immunity to ambient light [38]. On the other hand, the single-point scanner acquires the information point by point.

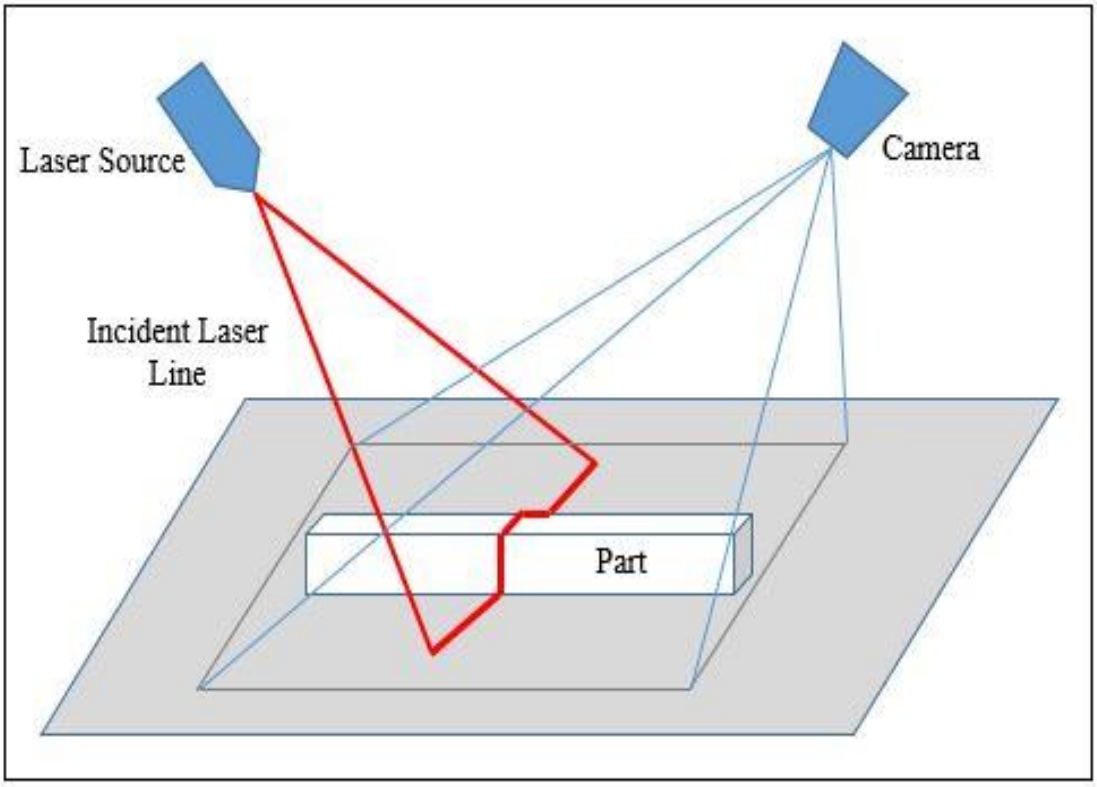

Figure 12: Slit Scanner

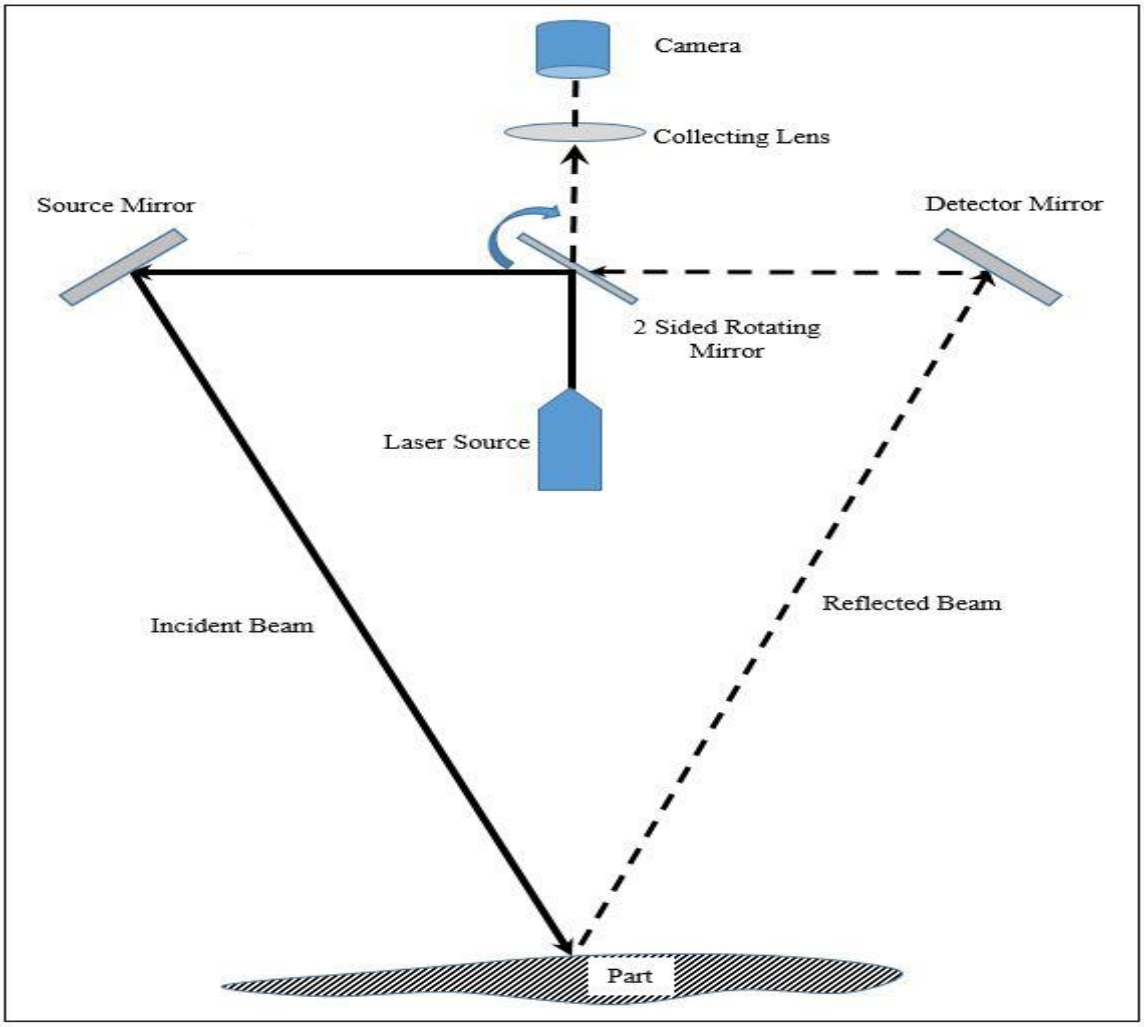

Figure 13: Single-Point Scanner

2.3.1.2 Passive Systems

The passive systems use shape-from-shading, shape-from-motion, or passive stereo vision to acquire 3D data [38]. Shape-from-shading employs a single camera for the part surface under different conditions. Depth information can be calculated by studying the changes in brightness over a surface and constraining the orientations of surfaces. Shape-from-motion utilizes motion sequence of the part by moving the part or the camera. Passive stereo

vision acquires 3D data by triangulation and uses two or more cameras to view the same part [38]. Passive systems in general are less sensitive to the environment, do not require any external energy source and can be used with mobile vision platform. Shape-from-shading and shape-from-motion are not suited for 3D data acquisition predominantly because of, sensitivity to the illumination and reflective properties of the part surface, limited ability to scan non-uniform surfaces and the difficulty in inferring absolute depth. Passive stereo vision systems have a problem of finding pixel correlations of two images. Hence, features need to be extracted and matched. Both extracting and matching are cumbersome and need intensive computation [38]. Table 2 lists various 3D data acquisition systems used in industry [38].

Table 2: Various Data Acquisition Systems Used in Industry

Manufacturer	**Type**	**Accuracy**	**Website**
Perceptron	Portable 3D scanner		http://www.perceptron.com
Kreon	Zephyr II Blue Laser Scanner	10µm	http://www.kreon3d.com/3d-scanners/zephyr-2-blue
Nextec	Hawk	2µm	http://www.nextec-wiz.com/hawk_specs.html
FARO	ScanArm Edge	25µm	http://www.faro.com/en-us/home
Polhemus	FastScan	762µm	http://www.polhemus.com/scanning-digitizing/fastscan
GOM mbH	ATOS 3D scanner		http://www.gom.com/metrology-systems/3d-scanner.html
Microscribe	Microscribe MX	50µm	http://www.3d-microscribe.com/MX%20Page.htm
NextEngine	Desktop 3D Scanner	127µm	http://www.nextengine.com/products
Steinbichler	Comet5		http://optotechnik.zeiss.com/en/products/3d-scanning/comet-l3d
Zoller+Fröhlich	Imager 5010X, 5010, 5006h		http://www.zf-laser.com/Home.91.0.html?&L=1
Konica Minolta	VIVID Series	50µm	http://www.3dscanco.com/products/3d-scanners/3d-laser-scanners/konica-minolta/

2.3.2 Development of 3D Scanners

Typical vision based systems produce a virtual representation of the part in the form of a dense point cloud. Multiple scans are necessary in order to thoroughly scan the part. This can be done in multiple scan passes by either changing orientation of the scanner or the part. Each point on the surface of the part corresponds to a unique point within this point cloud. This point cloud needs to be filtered and processed before any deductions are made from it so that extraneous points (reflections, dust, etc.) can be prohibited. The scope of this research is limited to the use of 3D scanning technology for measurement of surface roughness and for geometric inspection of additively manufactured parts. Hence, the development of 3D scanners for these applications has only been reviewed.

2.3.2.1 Development of 3D Scanners for Surface Roughness Measurement

Inspection of surface roughness is one of the important quality control processes that are usually performed to make sure that the manufactured part conforms to the design specifications. The earliest assessment of surface roughness was simply performed by running a fingernail across a surface. This technique survives to date as tactile comparison. The surface roughness is compared with a set of calibrated surfaces of known surface roughness and produced by the same process. These reference surfaces are often called comparators. A typical commercially available surface finish comparator is shown in Figure 14.

Figure 14: Surface Roughness Comparator

The study of surface topography actually became possible after the introduction of stylus profiling instruments in 1920s [40]. Surface roughness inspection is still widely done with the help of stylus instruments which correlate the motion of stylus tip to the surface of the part. Such stylus instruments need to make physical contact with the part surface which limits the measuring speed. Moreover, the readings obtained are based on a limited number of line samples which may not represent the whole surface. These instruments often need calibration during the measurement process and are hence prone to human errors. Therefore, the stylus type (contact type) instruments are not suitable for high-speed automated production lines.

Luk et al. developed a method of surface roughness measurement which could be integrated in a production line. This method was based on analyzing the patterns of white light scattered from the surface of the part. They used a microcomputer for analysis of the patterns obtained. The readings obtained were then compared with the readings from a stylus

instrument. Their findings suggest that the machine vision system they developed for surface roughness measurement was faster, more accurate, and had higher repeatability than the stylus instruments [41]. Koçer et al. investigated the performance of a non-contact surface roughness measurement system based on the principle of image processing. They took images of the part surface with the help of Leica Z6 Apo macroscope and obtained surface roughness values by image processing. The comparison of the readings from their system with the ones obtained from Mitutoyo Surftest SJ-201P profilometer shows that their system is not as accurate as the profilometer but the readings obtained from image processing were found to be in correlation with the profilometer [42]. Furthermore, researchers have also used Interferometry, CT, and Scanning Electron Microscope (SEM) for surface roughness measurement. However, none these methods are suitable for in-line measurement and require calibration frequently.

2.3.2.2 Vision-Based 3D Data Acquisition Systems for Geometric Inspection

Modern production lines cannot be established without using a number of imaging systems for monitoring and controlling the processes. These tasks must be automated as humans have a reported reliability of only 80% in repetitive assessment of products [43]. Hence, automated visual inspection systems have been widely used since 1980s [44]. Machine vision based inspection and quality control in industry has expanded remarkably since then [44]. In recent years, measurement, inspection, and quality control in industry have benefited from various 3D inspection techniques [45]. The increasing compactness to integrate these systems into the production line as well as decreasing costs have accelerated the use of 3D scanning techniques. Meeting the current demand for quality standards makes the use of these systems essential.

Aguilar et al. investigated the accuracy of different camera calibration and measurement methods used in 3D stereo vision system. They used the 3D stereo vision system in car frame measurements and reported that it was accurate up to 0.001 mm [46]. Molleda et al. developed a 3D inspection system based on triangulation technique for inspection of rolled metals. They report that the accuracy in their application is limited by the undesired movement due to vibrations of the rolled product and they used a low pass filter to remove noise generated from those vibrations [47]. Valeknburg et al. developed a structured light system for 3D measurement. This system had a reported accuracy of 0.3 mm [48]. Xu et al. developed a real-time 3D inspection systems for automotive parts based on structured light patterns. They inspected various automotive parts and reported an accuracy of 0.18 mm for their system [49].

Many researchers have used CT for part inspection [50], [51]. Over the past ten years, CT has started to migrate from medical applications to industrial applications. However, industrial metrology instruments need a different design and data analysis approach to produce measurements with high repeatability. Computed Tomography in today's world has revolutionized the industry by providing unique advantages in metrology of complex geometries. Due to such advantages, CT finds itself useful in a wide range of industries including electronics, automotive, aerospace, and biomedical industry. CT is being used for many inspection and testing tasks in the industry today where accuracy is of less importance. It has been mainly used for image acquisition and inspection although a few companies like General Electric (GE) and Nikon have developed industrial CT scanners which could be used for inspecting mechanical parts [52], [53]. It can be inferred from the above examples that there is no best technique (or instrument) that can produce accurate readings with high

repeatability in a dynamic environment. Hence, the abilities of a 3D laser scanner for use in metrology have been investigated in this research.

2.4 Chapter Summary

This chapter provides the reader with an overview of various additive manufacturing processes. The metal additive manufacturing processes, their limitations, and applications in the industry were outlined. Use of 3D scanning technology for part inspection in additive manufacturing is an area of particular interest to this work. A review of various methods and instruments used for data acquisition in metrology is presented. This chapter also describes various approaches adopted by the researchers for using vision-based 3D data acquisition techniques for measurement of surface roughness and geometrical inspection. Though there are many vision based systems on the market and are used in metrology, it has not been investigated if the nature of the part surfaces like the ones produced in additive manufacturing, affects the accuracy of vision based systems. From Table 2, it can be seen that the FARO laser scanner has an acceptable accuracy and it can turn out to be a powerful tool in metrology of AM parts. Hence, it is reasonable to investigate the abilities of 3D scanning.

CHAPTER 3

METHODOLOGY

To investigate the abilities and/or limitations of the 3D scanner, three representative parts were defined and several parameters were measured during this study. At first, the ability of the scanner to capture the variations in the surface texture of metal parts was investigated. The scanner was then used to measure the geometrical dimensions and tolerances on additively manufactured parts. Further, the implications of the rough surfaces produced by additive manufacturing on the measurements were explored. In these experiments, conventional measurement tools were also used to examine the performance of the 3D scanner.

This chapter describes the approaches used in pursuit of the research objective mentioned in Chapter 1. It starts with a brief overview of Average Surface Roughness (Ra) parameter and the methodology used to measure it using the 3D scanner in Section 3.1. Section 3.2 presents an overview of the test parts, the FARO 3D Scanner, the scanning procedure, and the data processing steps needed to be performed on the scan data. This discussion is followed by the methodology used to characterize the part features and the methodology used in GD & T analysis using Geomagic Qualify and a CMM in Section 3.3.

3.1 Investigation of the Ability of a 3D Scanner to Measure Average Surface Roughness

3.1.1 Average Surface Roughness (Ra)

Average surface roughness is defined as the average deviation of the surface profile from the mean line [54]. The equation for average surface roughness can be written as follows:

$$R_a = \frac{1}{L}\int_0^L |y(x)|\,dx \cong \frac{1}{N}\Sigma|yi| \quad \ldots\ldots\ldots\ldots\ldots\ldots \quad (1)$$

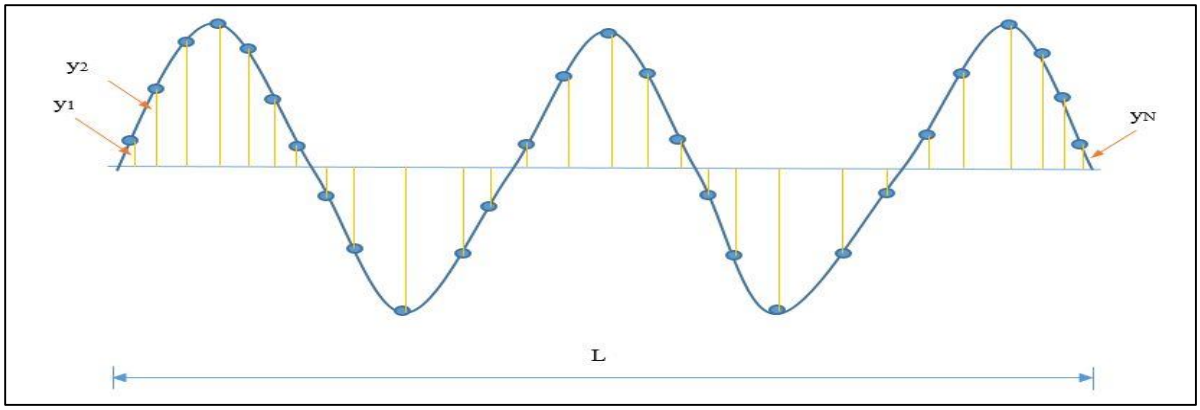

Figure 15: Surface Profile Example

As can be seen from equation (1), the average surface roughness can be determined by calculating the average of normal distances of the points from the mean surface line. An example of a surface profile is shown in Figure 15.

To investigate the ability of the 3D laser scanner for surface roughness measurement, various surfaces with known and estimated surface roughness were used in this experiment. Traditionally machined (ground, milled, turned) flat surfaces typically found on surface comparators as shown in Figure 16 were used to investigate the accuracy of 3D laser scanner. As this research is focused on additive processes, additiviely manufactured part surfaces were also used in this experiment. The average surface roughness of these additively manufactured surfaces was pre-determined with the help of a profilometer (Mitutoyo, Aurora, IL) as shown in Figure 17. The profilometers are often not efficient while measuring additively manufactured surfaces as they miss out on certain profile details. Hence, the experimental values of average surface roughness of EBM parts measured by Iquebal et al. using Nanovea M1 test platform [55] were used for reference.

Figure 16: Surface Comparator

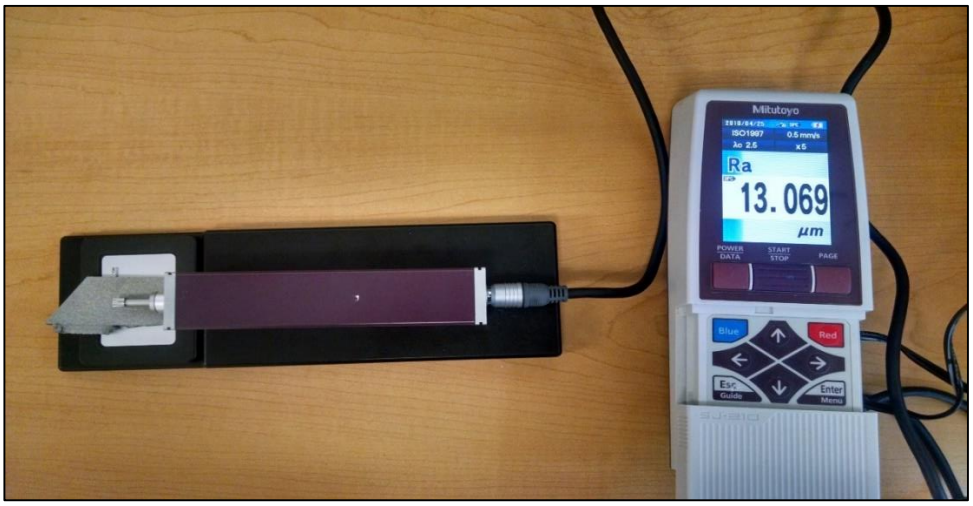

Figure 17: Surface Roughness Measurement with Profilometer

3.1.2 Determination of Average Surface Roughness using a 3D scanner

The part surface whose surface roughness is to be measured first needs to be scanned using the 3D laser scanner. For the purpose of the experiment conducted, the surface under observation was masked as showed in Figure 18a. The length between the maskings was kept commensurate with the maximum traverse length of the profilometer. The part surface was then scanned with the masking tape and the resulting scan obtained can be seen in Figure 18b. Figure 19 outlines the methodology used while determining Ra using the 3D laser scanner.

The scan was trimmed down to the green strip showed in Figure 18b to narrow down the measurement area and reduce the measurement error. The profilometer is a 2D measurement instrument as opposed to the 3D laser scanner which generates a point cloud for the whole part surface. The trimming procedure can be skipped for the parts having uniform surface variations like the surface comparator.

(a) (b)

Figure 18: Masked Part Surface (a) and Scan of the Part Surface (b)

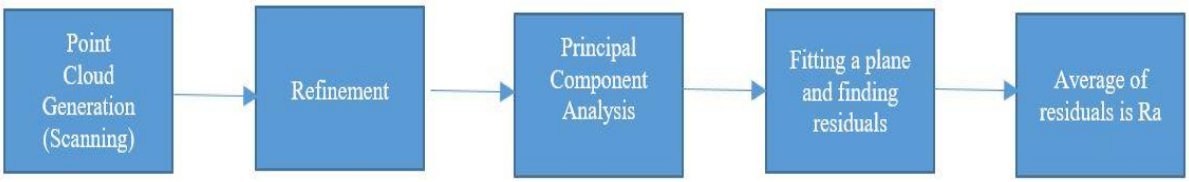

Figure 19: Methodology: Surface Roughness Determination

After trimming, the point cloud representing the scan was exported as a vertex file into a MATLAB code. The code is a procedural approach in which a plane is first fit through these points and the average of the normal distances (residuals) of the points from the fit plane is measured. This average distance is the required average surface roughness value. A very common method, least squares method, is often used to fit a regression plane through such data. In this case, least squares method cannot be used as the point cloud is randomly oriented in space and there is no clear distinction between the dependent and independent variables. Moreover, the least squares method does not minimize the orthogonal distances from the plane. It rather minimizes the distance from the plane to the point along any axis that we pick. Hence, the code utilizes a different method known as Principal Component Analysis (PCA) to find the response variable in the data. There are millions of points in a part's scan. It is always a challenge to determine the predictor and response variables by just looking at the data. PCA solves this problem by arranging the variables in the order of their respective variances. The one with the least variance can be treated as a response variable. Hence, it is appropriate to use PCA in this case. Figure 20 illustrates the fitting of a plane through the data that was obtained from the trimmed scan from Figure 18b. The points above the fit plane are marked in Green and the ones below the fit plane are marked in Red. After the plane is fit, the code automatically

measures the distances and outputs the average roughness value. This code can be found in Appendix 2.

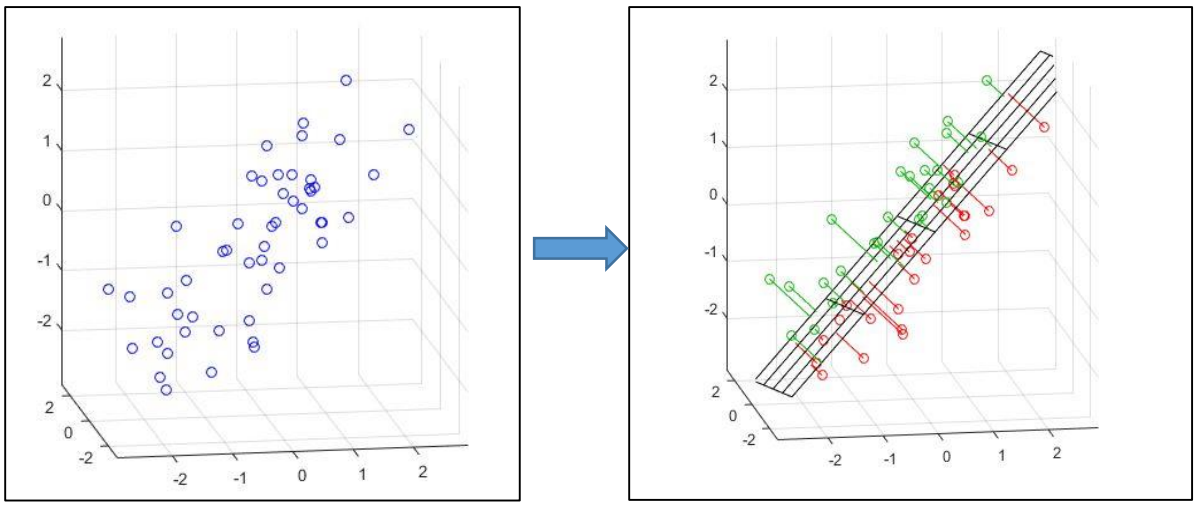

(a) (b)

Figure 20: Point Cloud (a) and Fit Plane (b)

3.2 Characterization of Additively Manufactured Metal Parts

3.2.1 Test Parts

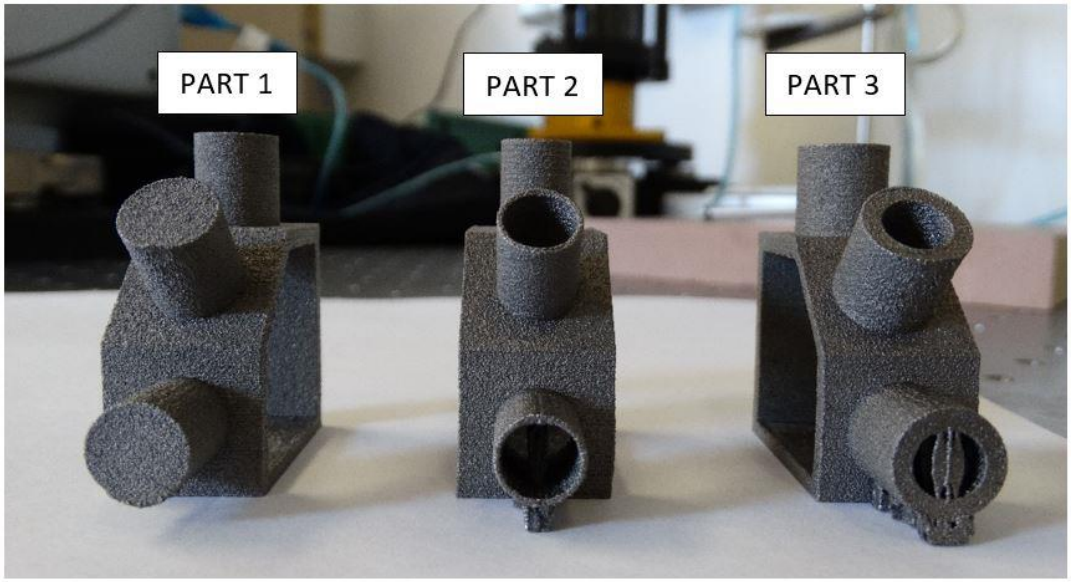

Figure 21: Test Parts

For this experiment, three test parts were designed and manufactured additively out of Ti6Al4V. These parts were built in an A2 (Arcam, Mölndal, Sweden) EBM machine and are dimensionally similar. Each part has three cylinders at three different angles: 0º, 45º, 90º. The protruding cylinders on each of them have different diameters and wall thickness. The difference in the diameters of these cylinders was intentionally introduced to examine if there are any deviations from the CAD model in the manufactured part because of any particular geometry. The support structures were removed using pliers. Some supports could not be removed manually and were ignored during the analysis. The manufactured parts and the respective part numbers are shown in Figure 21. These part numbers will be used to refer to these parts hence forth.

3.2.2 FARO Edge 3D Scanner

Figure 22: FARO Edge Scanner

The FARO Edge 3D laser scanner (FARO, Lake Mary, FL) shown in Figure 22 was used to generate the scans of the parts. This scanner is a 7-axis, articulated arm with a spherical working volume. Every joint has a rotary optical encoder. The signals from these encoders are processed using advanced error coding and temperature compensation technology. The positional data of the scanned part is sent to the host computer using either wired or wireless modes of communication [56]. The scanner has a built-in functionality by which different exposure algorithms can be selected while scanning different types of parts. It includes the Automatic- Metal Reflective algorithm, meant for unpainted, raw, metal parts and was used for scanning purposes throughout this study.

3.2.3 Point-Model Generation

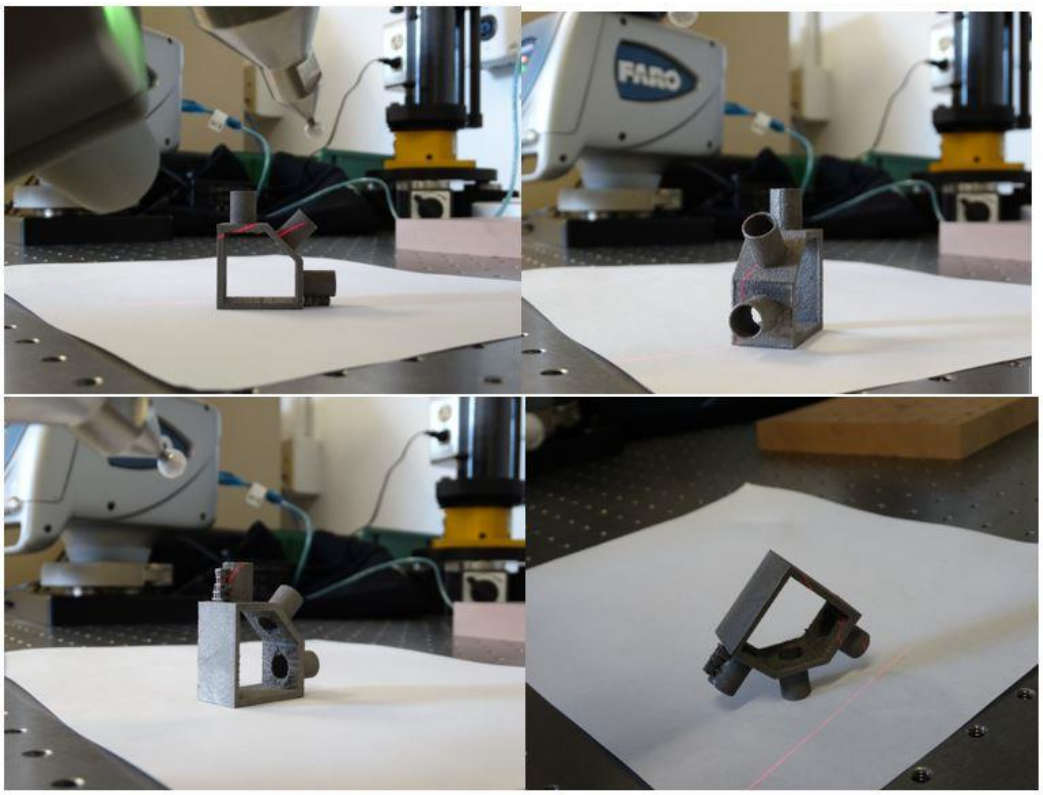

Figure 23: Part Orientations used while scanning

The parts needed to be scanned in different orientations to capture all the details. Thus, in the experiment, every part was scanned in four different orientations as shown in Figure 23. A dulling spray was used on the parts before scanning to reduce reflectivity and the resulting noise. ***Geomagic Studio*** (3D Systems, Rock Hill, SC) was used as the scanning platform and scans were taken in groups with a separate scan group for each of the scanning orientation. Saving the scans in groups helps to identify the different orientations while registering the scans with respect to each other.

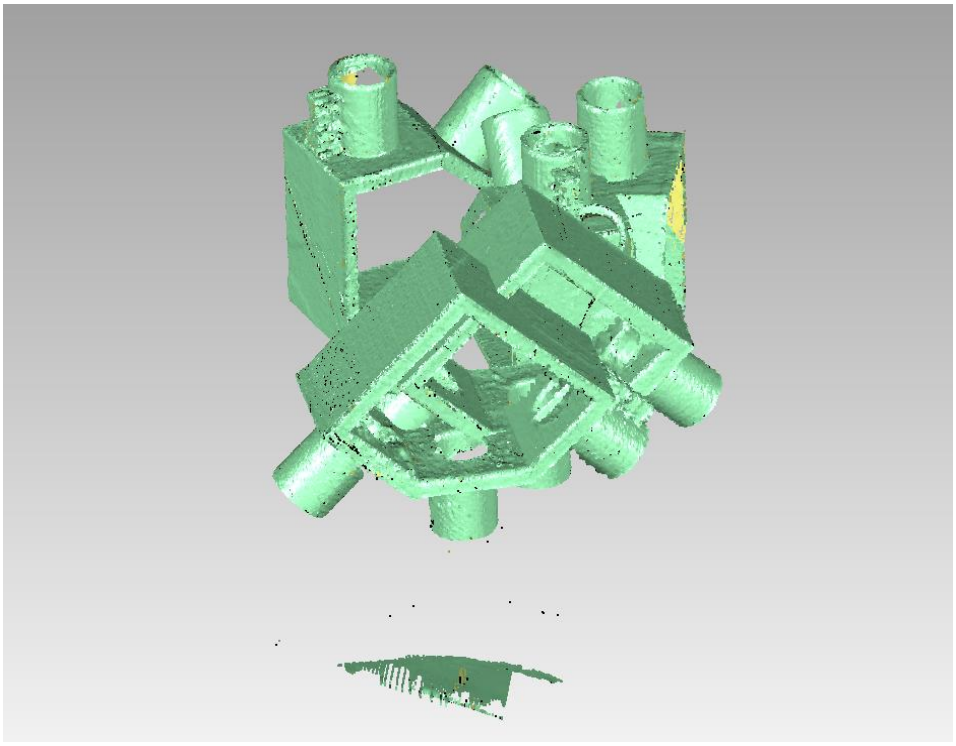

Figure 24: Raw Scans

Figure 24 shows raw scans typically achieved after multiple scan passes. The scans are randomly oriented and need to be registered to get a complete point-model of the part. For aligning the scans, the *Manual Registration* tool from Geomagic Studio was used which allows

the user to create a rough registration of two or more overlapping scans by defining corresponding points in overlapping regions [57]. After a rough registration is created, *Global Registration* is performed to refine the registration. The registered groups of scans are then converted into a single point object to perform filtering operations. This single point object is then analyzed for presence of any outliers (points at a certain distance from most other points) which are deleted later.

A grid filter is then used to reduce the number of points in the point-model. The grid filter creates an evenly spaced set of points, regardless of curvature and original density. It retains a point that is closest to the center of each grid cell in a certain sample. The grid spacing in this filtering process is the average spacing between all of the selected points. Figure 25 shows a complete point-model obtained after registering and filtering the scans.

Figure 25: Combined Point-Model

A point-model for each of the three test parts were created as explained in this section for further analysis. The following section describes the utilization of these point-models for GD & T.

3.3 GD&T Analysis

The point-models obtained were used to determine the geometrical accuracy of the parts using Geomagic Qualify. The Geomagic Qualify is a 3D metrology software by Geomagic which allows the user to import a CAD model of the part and compare it with the scanned point-model. This comparison effectively gives the information about the part geometry and feature tolerances.

The above process can be explained with the help of the following block diagram.

Figure 26: Methodology- GD & T Analysis

When the CAD model and the point-model of the part are imported in Geomagic Qualify, the point-model appears at a distant location, unaligned with respect to the CAD model.

Figure 27: Unaligned point-model and CAD model in the same space

As shown in Figure 27, the yellow model represents the imported CAD model whereas the grey model represents the point-model. The alignment is achieved through the *Best Fit Alignment* command which operates in two phases. The first phase is an initial gross alignment

in which the models are aligned roughly based on a lower number of points of comparison. This initial gross alignment can be bypassed if the objects are already roughly aligned. In the second phase of *Fine Adjustment*, the alignment is optimized using a higher number of points of comparison. The aligned models are shown in Figure 28 where the red dots represent the point-model.

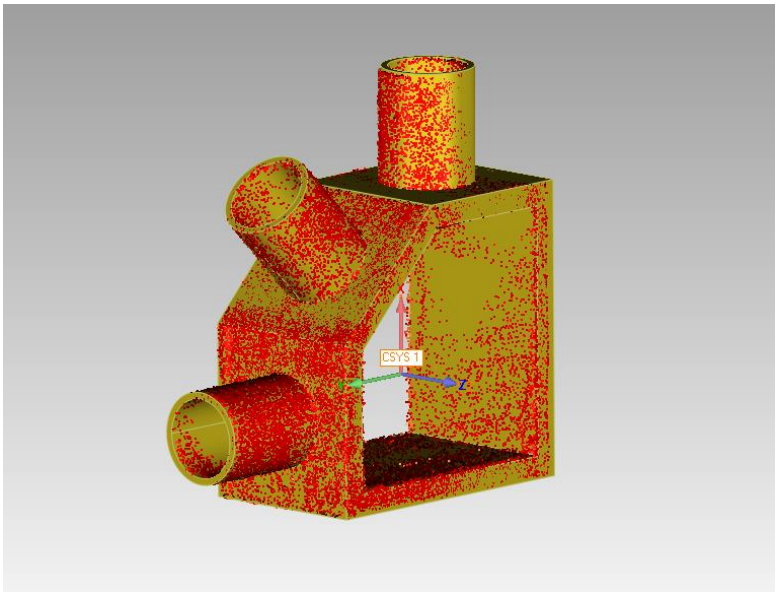

Figure 28: Aligned CAD and points models

After aligning the models, features were defined on both models for further analysis. Firstly, the *Quick Feature* command was used to define planes and cylinders on the CAD model. As the scanner fails to reach all the points representing the inner cylinder, for hollow cylinders, only the outer cylinder was defined. These features were then transferred to the point-model so that an inspection regimen can be performed. The features defined on both the CAD model and the point-model are shown in Figure 29. The co-ordinate system in Figure 29

is the one in which the CAD model was designed. Figure 29 (b) shows the point-model where the build direction is represented by the Y-axis.

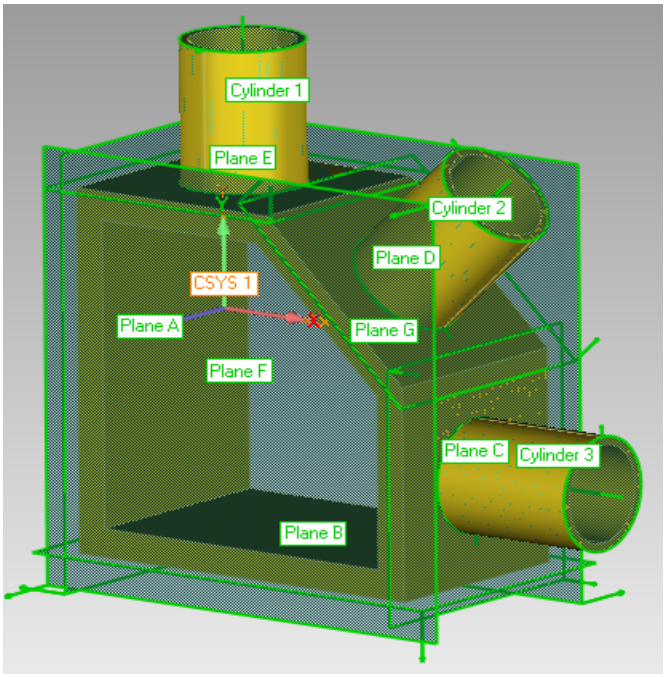

(a) CAD Model

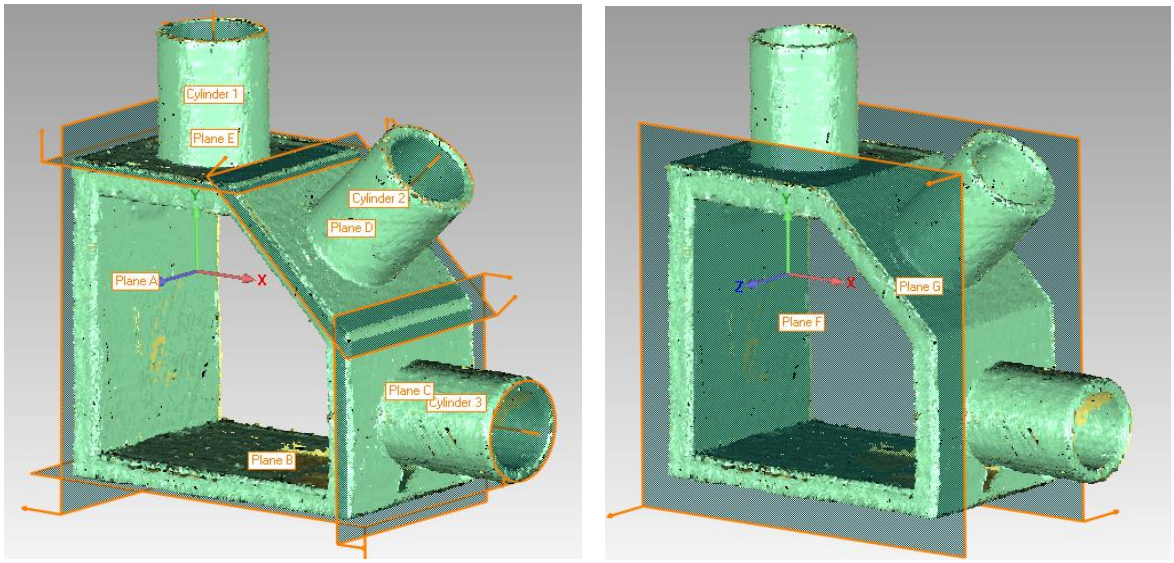

(b) Point-model

Figure 29: Defined Features

A total of ten features including seven planes and three cylinders were defined on both models. Each of the features were identified by a unique name as shown in the above figure. Following dimensions and tolerances were recorded using GD & T tools in Geomagic Qualify:

Table 3: Measured Dimensions and Tolerances

Dimension	**Features Involved**
Length	Plane A, Plane C
Height	Plane B, Plane E
Width	Plane F, Plane G
Angle	Plane A, Plane B
Angle	Plane B, Plane C
Angle	Plane B, Plane D
Angle	Plane A, Plane E
Angle (w.r.t. fixturing plate)	Cylinder 1
Angle (w.r.t. fixturing plate)	Cylinder 2
Angle (w.r.t. fixturing plate)	Cylinder 3
Diameter	Cylinder 1
Diameter	Cylinder 2
Diameter	Cylinder 3
Tolerance	**Feature Involved**
Flatness	Plane A
Flatness	Plane B
Cylindricity	Cylinder 1
Cylindricity	Cylinder 2
Cylindricity	Cylinder 3

The whole process from characterizing the part to GD & T analysis, as explained above, was repeated four times for each of the three parts.

To compare the results obtained using the 3D scanner with a conventional instrument, all the parameters listed above were also measured using a CMM. A Sheffield Metrology CMM (Hexagon Metrology, Stockholm, Sweden) equipped with a probe (Renishaw, Gloucestershire, UK) having a diameter of 4 mm was used in this study.

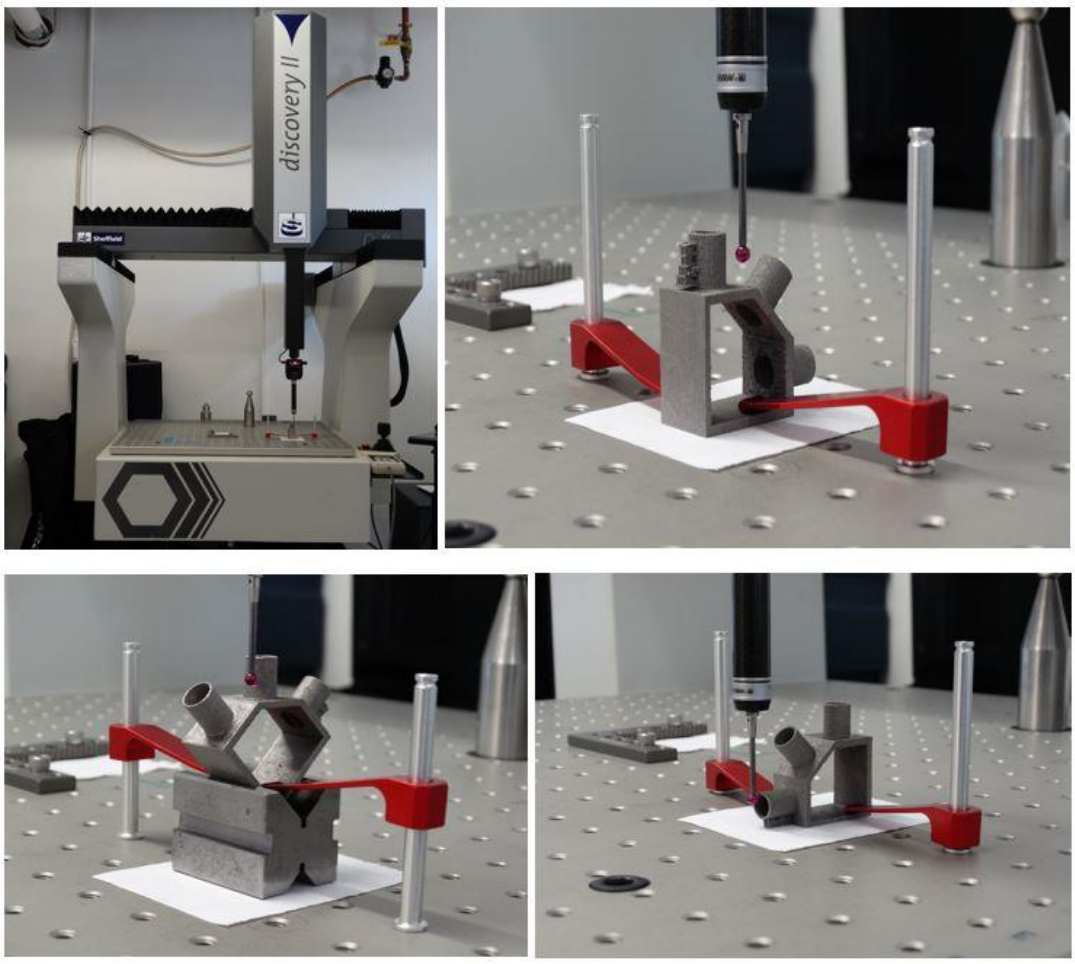

Figure 30: Part Orientations and Fixturing during CMM Measurements

As can be seen from Figure 30, the parts were held onto the CMM plate in appropriate positions using the commercially available CMM fixtures. While measuring a cylinder using a CMM, it is required to take the first three points in a plane perpendicular to the axis of the

cylinder [58]. Therefore, a v-block was used while measuring cylinder 2 to ensure the perpendicularity with respect to the CMM plate. Twenty points were taken manually to define the critical features whose tolerances were to be measured. For all the remaining, the number of points taken was at least twice the minimum number of points required to define a feature. PC-DMIS, a software from Hexagon Metrology was used for data processing throughout the CMM measurements. All the dimensional measurements in this study were based on ASME Y14.5 GD & T standards. The 3D scanner and CMM measurements were then compared to each other and also to the nominal CAD dimensions to investigate the deviation from the design specifications.

3.4 Chapter Summary

The experiments performed in this study were explained in detail in this chapter. The chapter begins with a description of the approach to determine the surface roughness using the 3D laser scanner. A brief introduction to the test parts designed and additively manufactured for GD & T inspection during this study was presented. A procedural approach to scan the parts, process the data obtained from the scans, and analyze the data was described. Then the different parameters that were measured in this study were described and the chapter ends by outlining the analysis that was carried out on the obtained measurements. The results obtained from this study are presented in the next chapter.

CHAPTER 4

RESULTS AND DISCUSSION

This chapter focuses on the results obtained after implementing the procedures explained in the previous chapter. It begins with the results obtained from the investigation of the limitations of surface roughness measurement using the FARO scanner. This is followed by the results obtained from the GD & T analysis of the test parts.

4.1 Surface Roughness Measurement

The surface roughness measurements were done on four different surfaces having different surface textures. The range of average surface roughness values of these surfaces was from 2.97 µm to 32 µm. The results obtained from this experiment are as follows:

1) Standard Profilometer Calibration Plate:

Figure 31: Profilometer Calibration Plate

Table 4: Measured Surface Roughness on the Profilometer Calibration Plate

Profilometer (µm)	3D Scanner (µm)
2.97	17.034
2.97	8.8392

Figure 31 shows the least average surface roughness measured in this experiment. This surface is a standard, precision-machined, calibration plate. Such surfaces are typically used while calibrating the profilometer. As can be seen in Figure 31 and Table 4, the average surface roughness of this plate was 2.97 µm. The profilometer measured this value accurately. However, the 3D scanner failed to measure this value. The difference between the values in Table 4 can be attributed to the accuracy of the 3D scanner which is on the order of 25 µm. Hence, the scanner fails to capture the surface variations of less than 25 µm.

2) Surface Roughness Comparator:

Figure 32: Surface Roughness Comparator

Table 5: Measured Surface Roughness on the Surface Roughness Comparator

Profilometer (µm)	3D Scanner (µm)
12.5	25.4
12.5	23.4
6.3	30.001
6.3	25.69

A total of 4 surface patterns as shown in Figure 32 were used for surface roughness measurement. Table 5 lists the results hence obtained. As can be seen from Table 5, the 3D scanner again failed to read the surface roughness values because of the same reason as explained above.

3) EBM Part

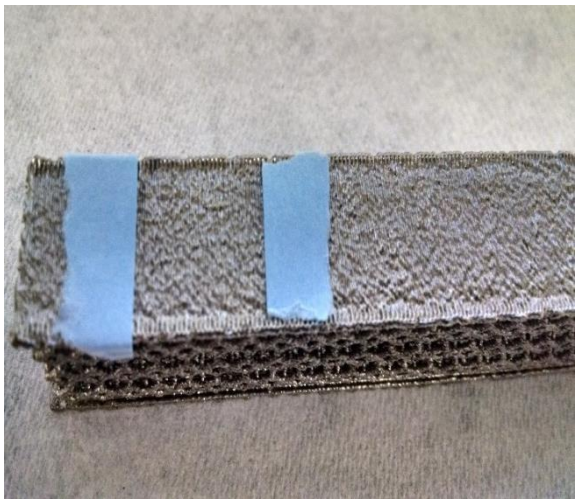

Figure 33: EBM Part Surface

Table 6: Measured Surface Roughness on the EBM Part

Profilometer (µm)	3D Scanner (µm)
31.923	55.88
29.33	53.34

An EBM part as shown in Figure 33 was used in this experiment to investigate how the scanner measures additively manufactured surfaces. It is evident from the first column of Table 6 that the additively manufactured surfaces have a non-uniform surface texture. Such surfaces lead to noise generation during scanning. It is difficult to capture all the details on the additively manufactured surfaces using the 2D profilometers. However, a 3D representation of the surface generated using the FARO scanner could potentially be near to accurate for measurement of surface roughness of the additively manufactured surfaces. Hence, the values in the second column of the Table 6 could actually be a better estimate of the average surface roughness.

4) EBM Test Parts

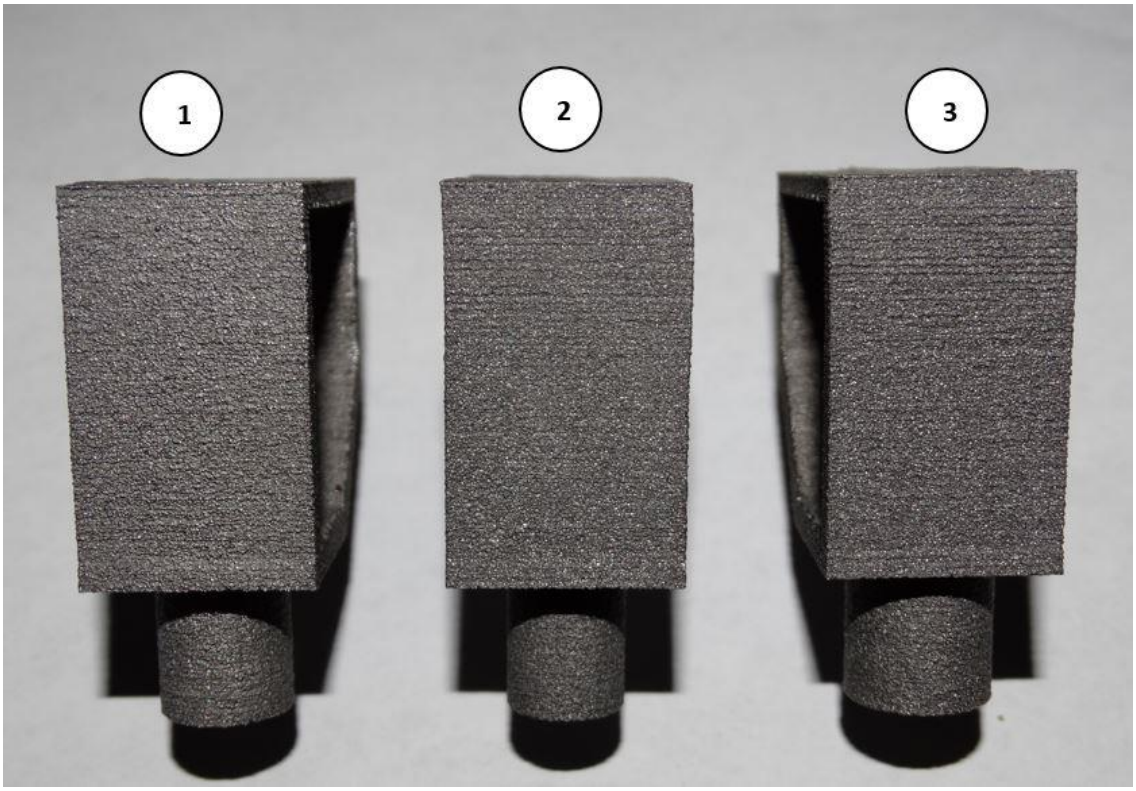

Figure 34: EBM Test Parts- surfaces used for roughness measurement

For each of the above surfaces, the average surface roughness determined using the 3D scanner was compared to the values obtained from a recent study by Iquebal et al. In this study, the surface roughness of EBM parts was measured using a Nanovea optical profilometer [55] where the surface roughness measured in the Z-direction (build direction) was 28.34 µm. Table 7 shows values of the surface roughness (in Z-direction) of the test parts.

Table 7: Measured Surface Roughness on the EBM Test Parts

Part	3D Scanner (µm)
Part 1	38.1
Part 2	25.8
Part 3	31.4

As can be seen in the above table, the values obtained using the 3D scanner were comparable to the values obtained from the optical profilometer. The variation in the average surface roughness between the test parts can be observed in the Figure 34.

4.2 GD & T Analysis

This section details the analysis of various linear, angular, radial measurements, and tolerances performed on the test parts. Section 4.2.1 describes the defects observed in the test parts followed by the dimensional and tolerance measurements performed during this experiment. Only one sample of each of the three test pieces was measured in this study. Hence, no statistical inferences could be drawn from the measurements.

4.2.1 Visual Inspection

Some defects were detected in the manufactured test parts after initial visual inspection. These defects are listed as follows:

1) Edge Extension

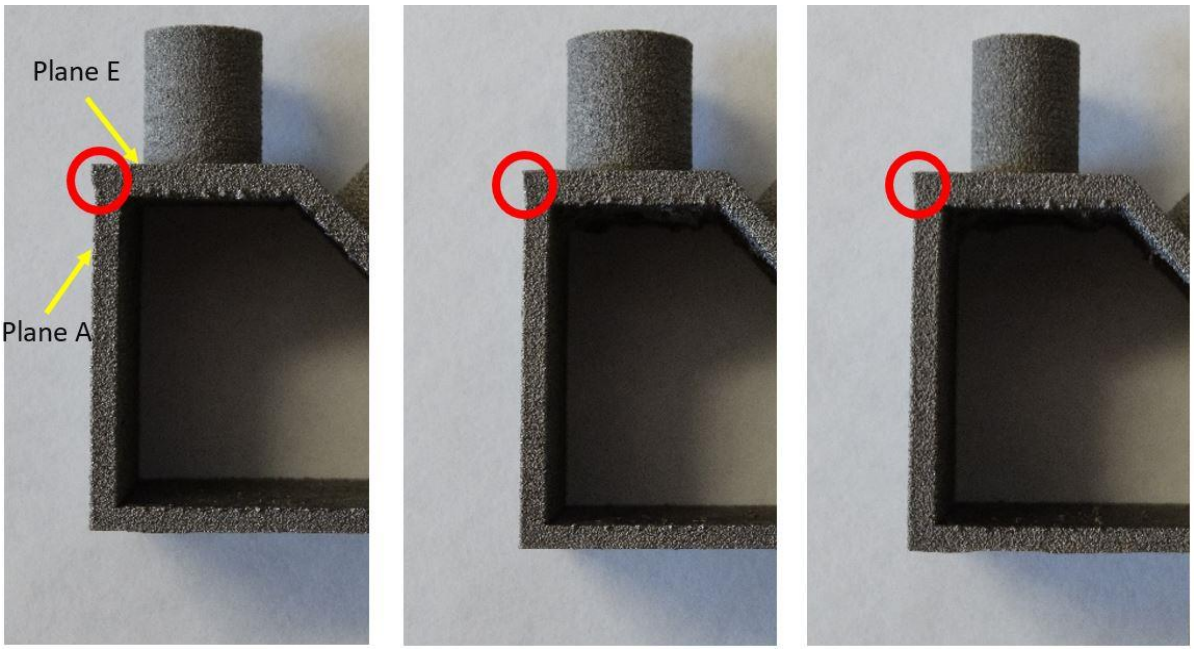

Figure 35: Defects-extended edges

As is evident from the above picture, the edge where plane A and plane E intersect was slightly extended in all the three test parts. Also, it can be observed that the edge extension was more prominent in part 1. This extended portion of the surface affects the flatness measurements. For the surface roughness measurements, this portion of the surface was excluded.

2) Bottom Surfaces

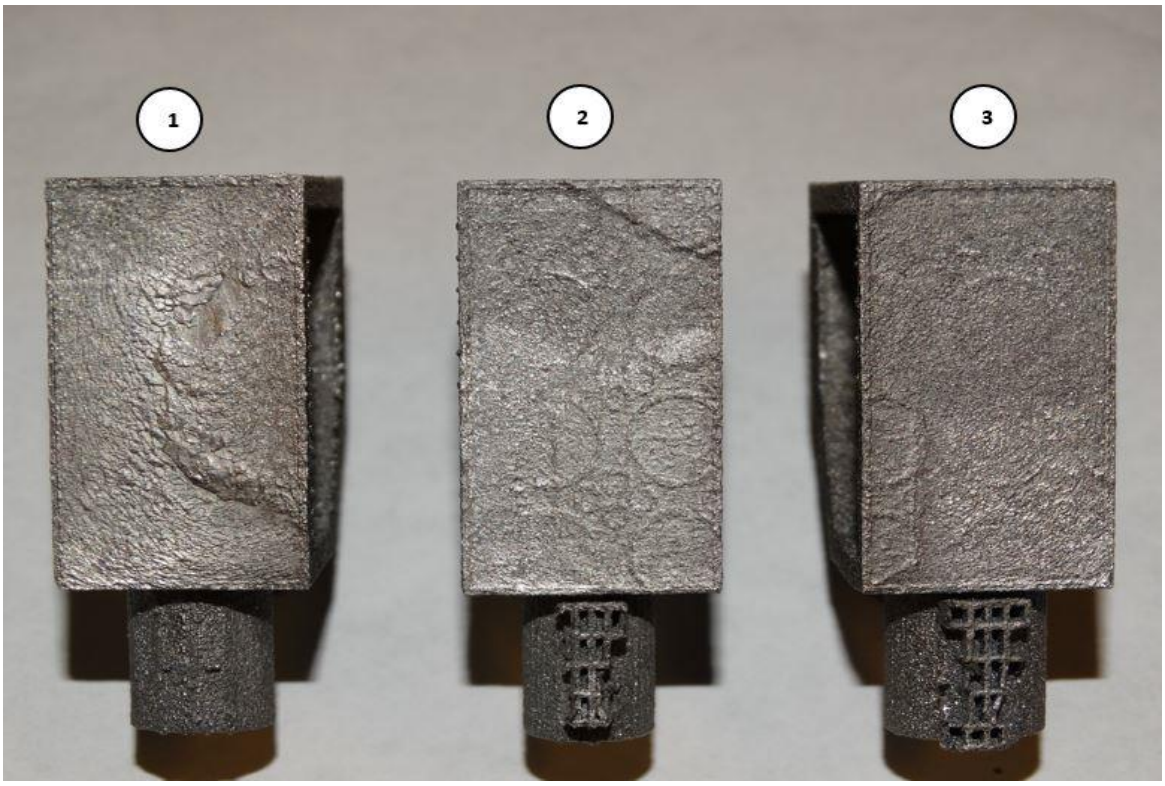

Figure 36: Defects: Bottom Surfaces

Figure 36 shows the bottom surfaces of the test parts. It can be seen that all the three surfaces were irregular and had impressions of the build platform on them. This significantly affects the flatness tolerance on these surfaces. As can be seen in the above picture, part 3 appears to have the least surface variations on the bottom surface.

3) Cylinder Distortion at 45º

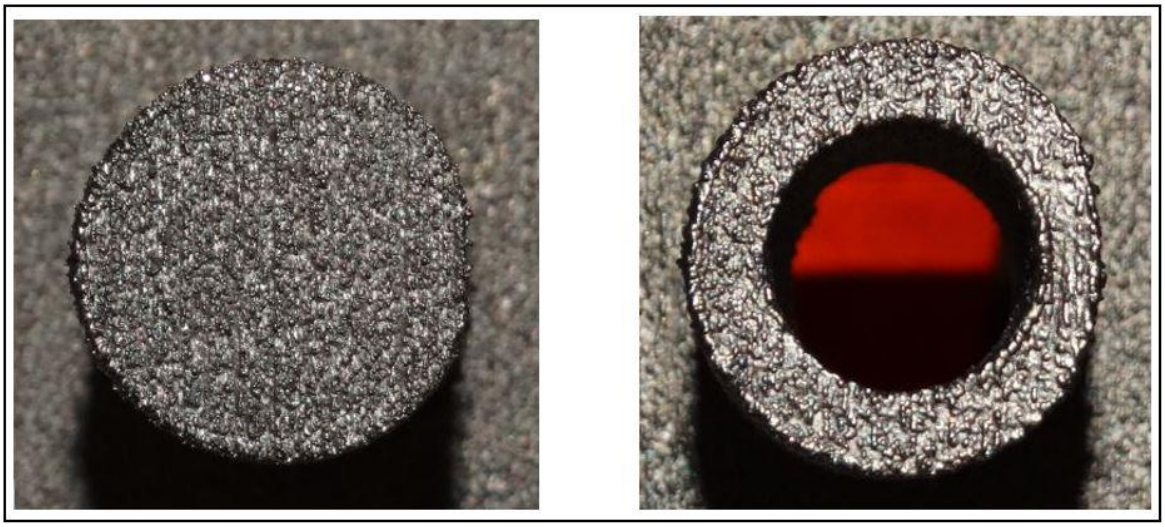

Figure 37: Defects: Cylinder Distortion

The cylinders at 45º in part 1 and part 3 were found to be distorted as can be seen in the above picture. These cylinders were flattened from the bottom.

4) Cylinder Distortion at 0º

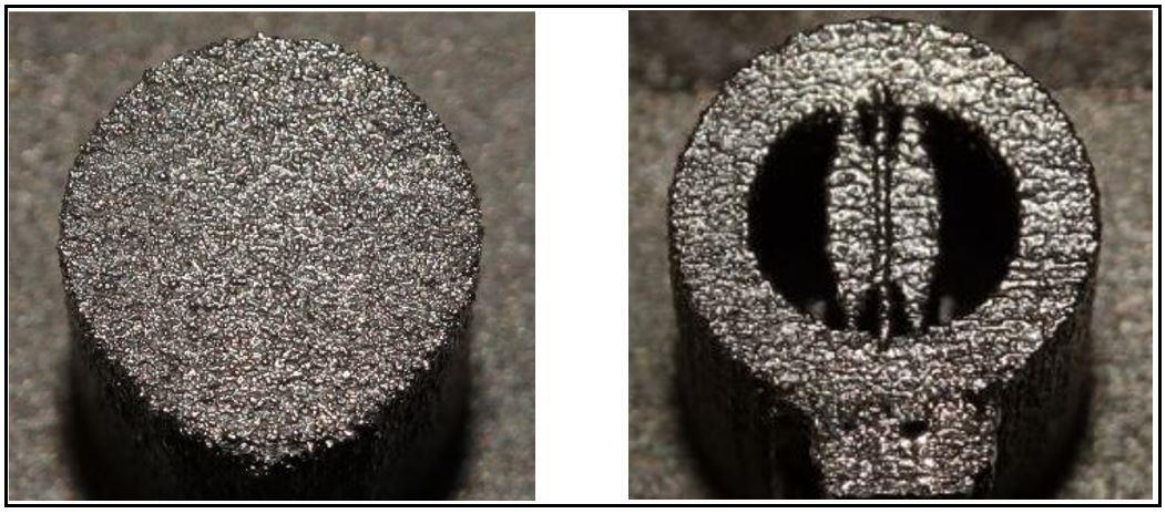

Figure 38: Defect: Cylinder Distortion

The cylinders at 0º on part 1 and part 3 were found to be ovalized and a significant distortion was also observed on part 1.

4.2.2 Dimensional Measurements

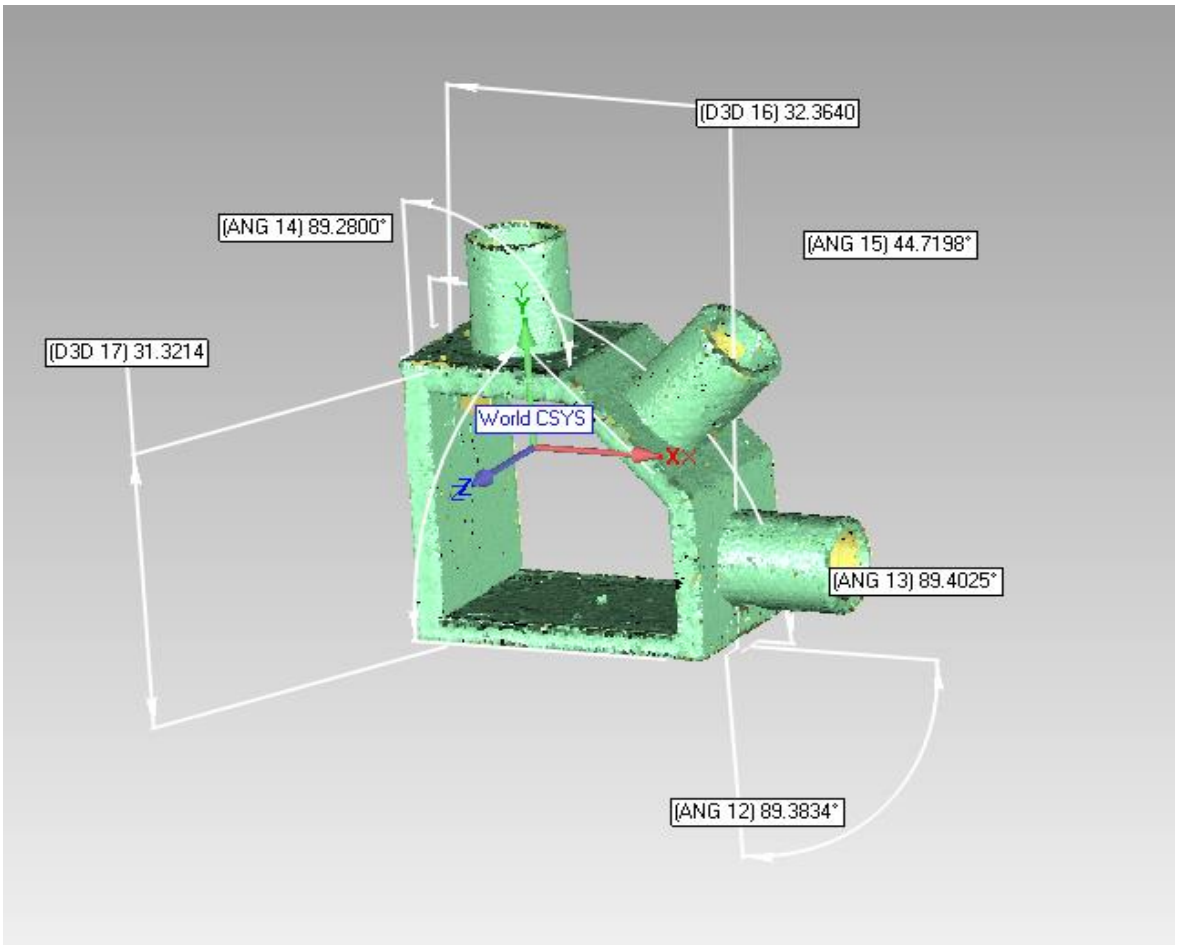

Figure 39: 3D Dimensioning in Geomagic Qualify

Figure 39 shows a typical 3D dimensioning tool in Geomagic Qualify which can be used to measure feature-to-feature dimensions. As similar results were obtained for all the measurements across all the test parts, only the results of Part 2 are shown. The results of the other parts can be found in Appendix 3.

4.2.2.1 Linear Dimensions

Basic linear dimensions of the part (excluding the height of the cylinders) were measured using both the CMM and the 3D scanner. To illustrate the results, a comparative bar graph is presented below.

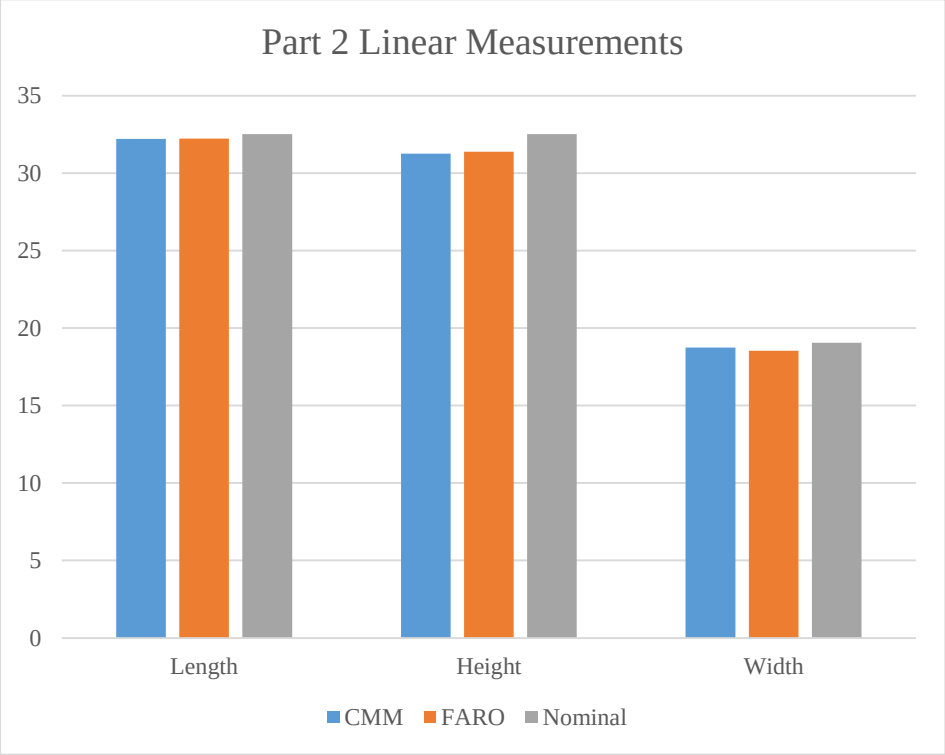

Figure 40: Linear Dimensions

From Figure 40, it can be said that there is no significant difference (2%) between the measurements obtained using the 3D laser scanner and the CMM. However, the linear dimensions measured above were a little shrunk when compared to their nominal (CAD) values. The average of shrinkage in the above parameters was measured across all the three parts and it has been reported in the following table.

Table 8: Percentage Shrinkage

Direction	% Shrinkage
X (Length)	1.28
Y (Width)	1.66
Z (Height)	3.77

This shrinkage can be attributed to the improper selection of the build parameters. The ARCAM machines come with a functionality where the user specifies the extra material to be added on the part to compensate for the shrinkage during the build. Hence, usually, the parts built on ARCAM's EBM machines are not expected to shrink.

4.2.2.2 Angular Measurements

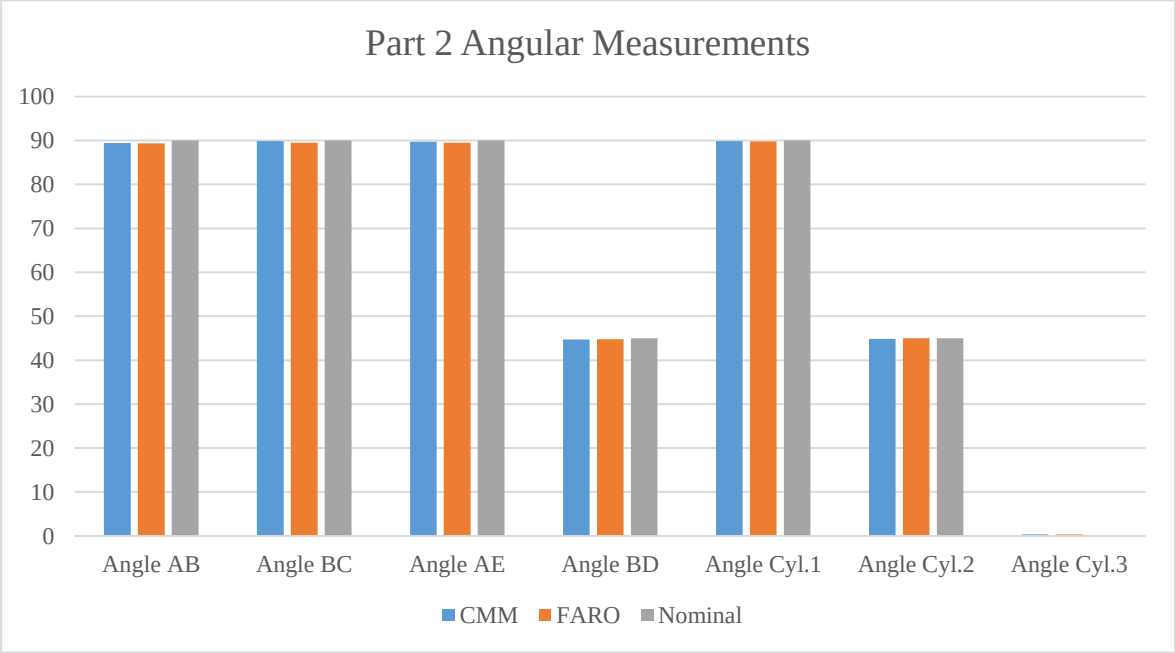

Figure 41: Angular Dimensions

Angular measurements were performed on all the outer surfaces and the cylinders of the test parts. The angles between the planes characterized as explained in Chapter 3 were

measured. For the cylinders, the angles of their axes were measured with respect to the flat measurement plates on which the parts were mounted. These measurements were performed to better understand the location of the cylinders. The results are shown in the above bar graph. As can be seen from the graph, the angular measurements using CMM and 3D scanner were within 2% of each other. There was a slight deviation from the nominal values of the angles and it was not more than 2% for any of the angles.

4.2.2.3 Radial Dimensions

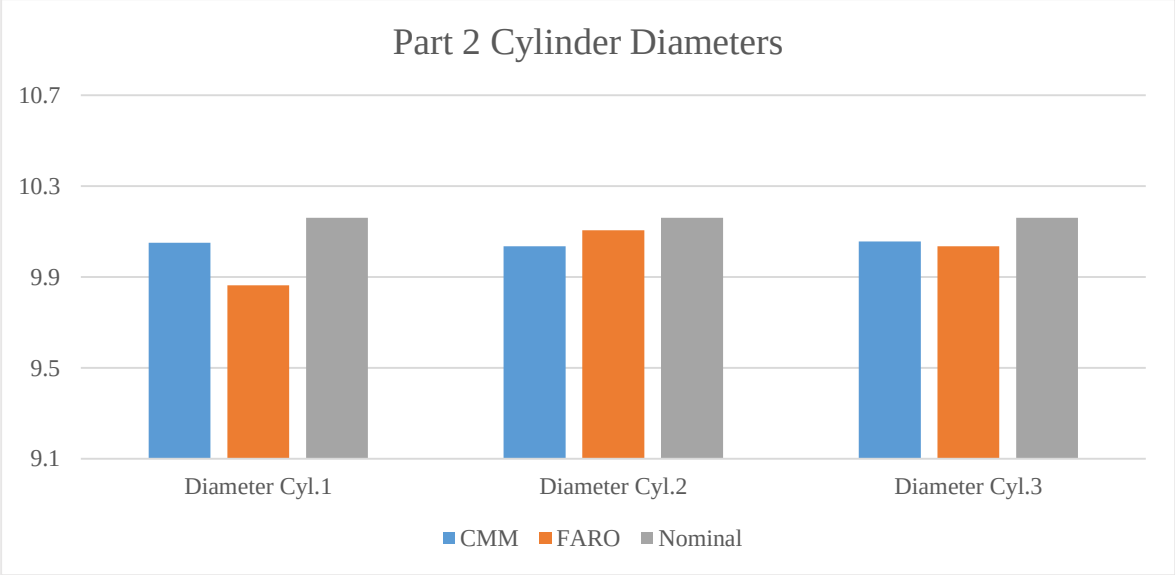

Figure 42: Diameters

Figure 42 shows a comparative chart of the diameters of the three cylinders on part 2. As can be seen in the figure, the diameters measured by both the CMM and FARO were within 2% of each other. The diameters of the cylinders were shrunk compared to the nominal values.

4.2.3 Tolerances

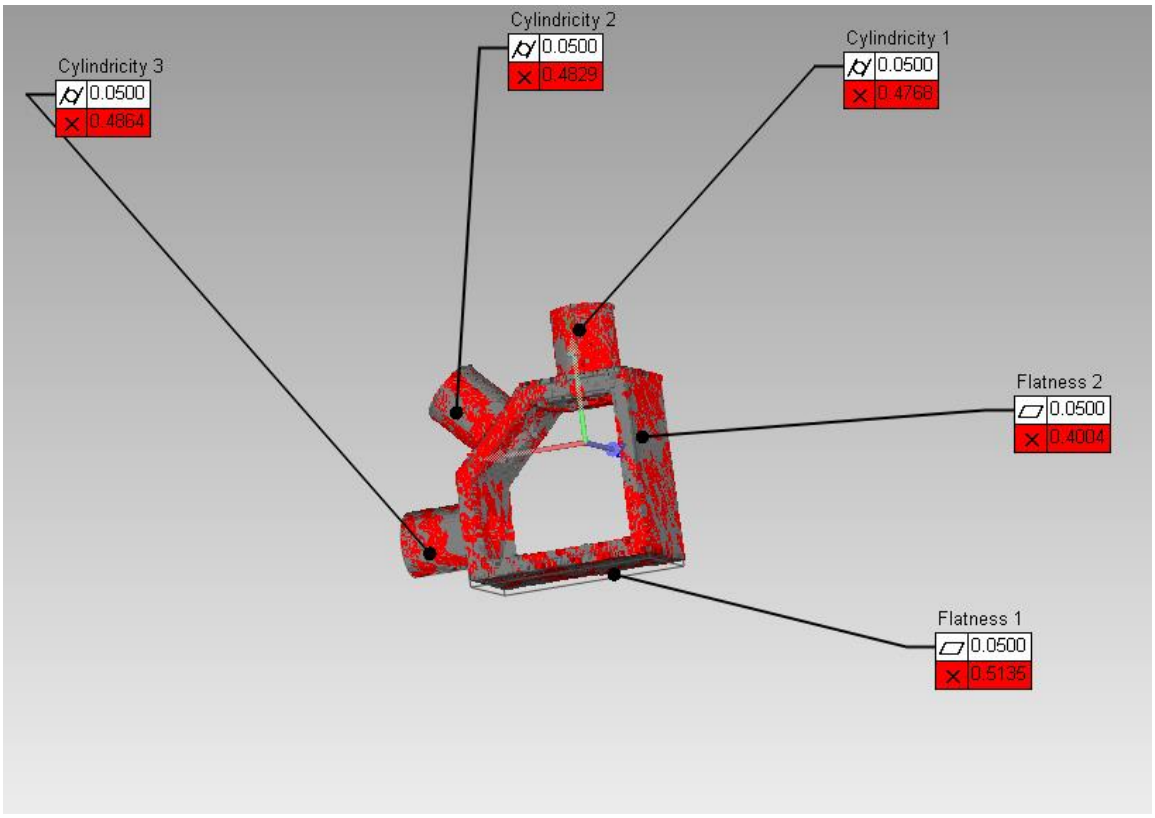

Figure 43: Geomagic Qualify GD & T Analysis

Figure 43 shows a typical Geomagic Qualify GD & T analysis window. The user has to first specify the nominal tolerance in order for Geomagic Qualify to evaluate the same tolerance on the test model. The tolerance value of 0.0500 is the default value set in the software. This value can be changed according to the design specifications and Geomagic Qualify marks the tolerance call-outs in Red (fail) or in Green (pass) according to the observed tolerance on point-model. The values obtained can be found in Appendix 3.

1) Flatness

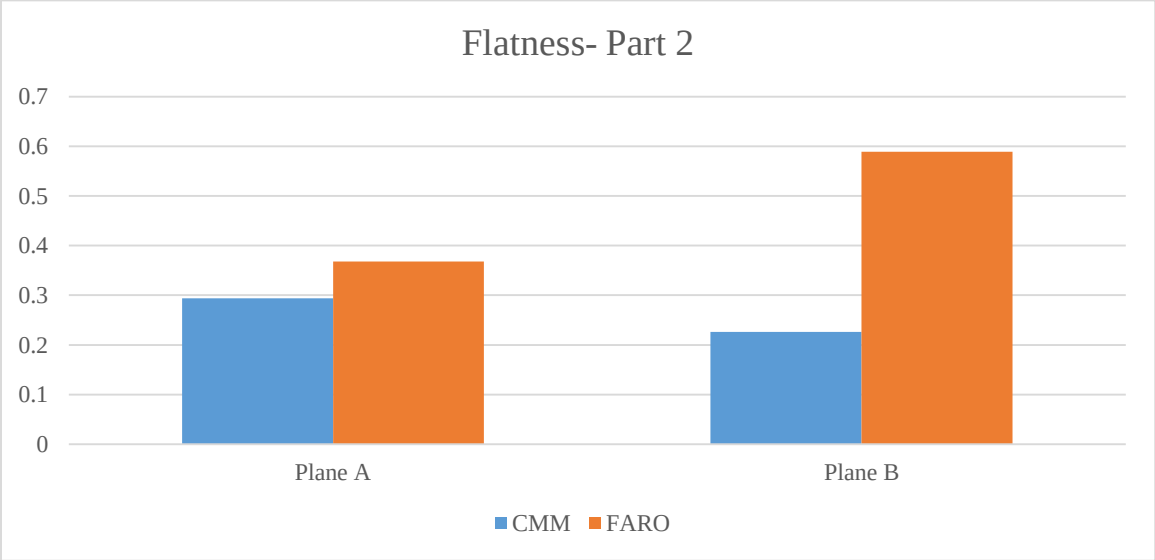

Figure 44: Flatness- Part 2

Figure 44 shows a bar graph of the flatness values of plane A and plane B measured using both the CMM and the FARO scanner on part 2. As can be seen in Figure 44, the tolerance values obtained using the CMM were always less that those obtained using the FARO. The primary reason behind this difference is the number of points. When the planes were characterized using the CMM, only 20 points were taken manually. On the other hand, the scanner captures thousands of points on the same plane. Considering the additively manufactured irregular surfaces, a validation study was done in order to justify this difference between the two instruments. In this study, the number of points taken was increased from 20 to 100 and it was found that the value of flatness for a plane increases with the number of points taken. Moreover, from the difference between the flatness values of plane B (see Figure

29) obtained using CMM and FARO scanner, it can be said that the CMM fails to capture all the surface irregularities.

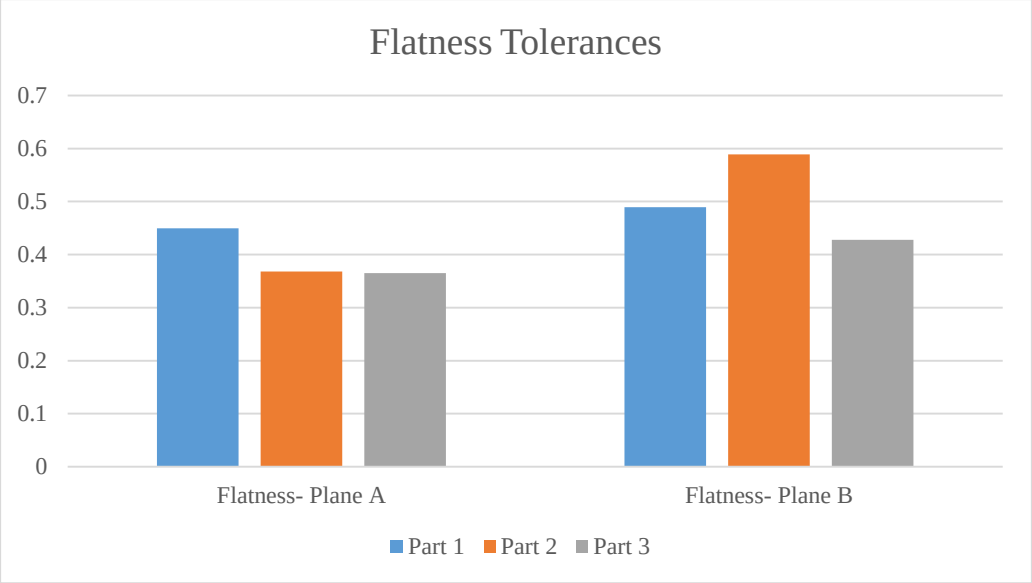

Figure 45: Flatness Tolerances

Figure 45 displays the flatness tolerances measured across all the parts. The visible irregularities on the bottom surfaces were well captured by the scanner. The tolerance measured on the bottom surface of part 3 was the smallest of the three parts. The prominence of edge extension observed in part 1 is evident in the above figure in terms of the flatness value of plane A (see Figure 29).

2) Cylindricity

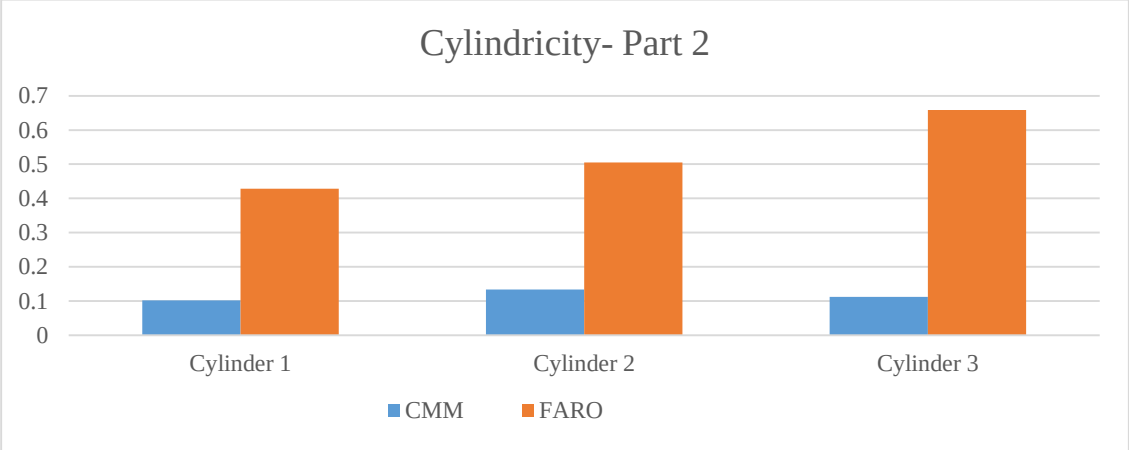

Figure 46: Cylindricity- Part 2

Figure 46 graphically represents the cylindricity tolerances measured on part 2. As can be seen in the figure, the difference in the values obtained using the CMM and the FARO worsens when compared to the flatness values.

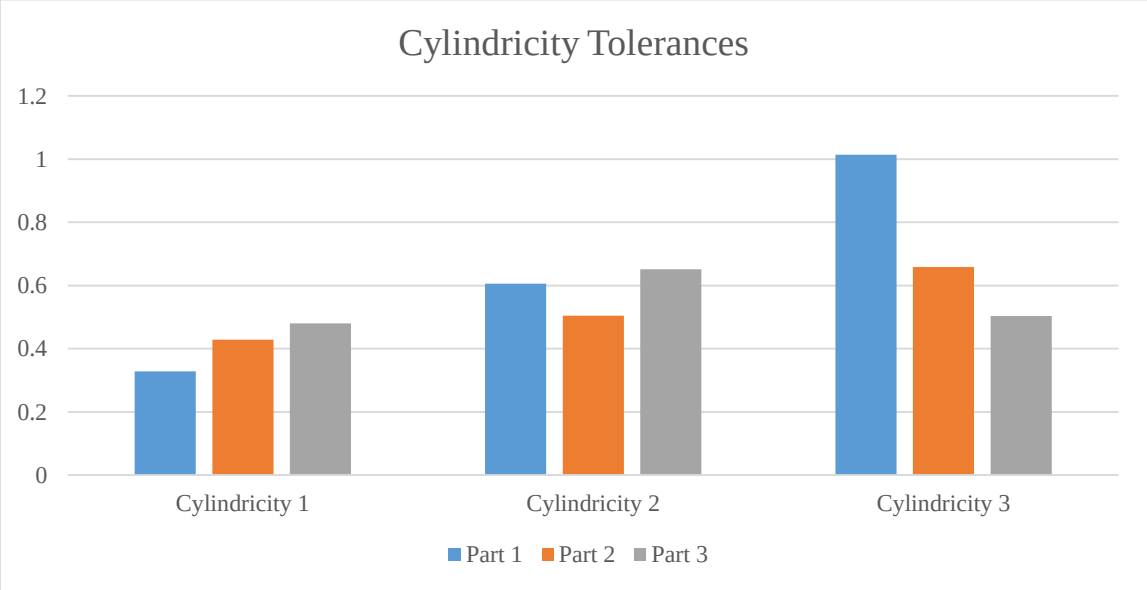

Figure 47: Cylindricity Tolerances

Figure 47 displays the cylindricity tolerance measured across all the parts. As can be seen in Figure 47, the cylinder 1 on each part had the least cylindricity. It can be said that the cylindricity (distortion) increases from cylinder 1 to cylinder 3 i.e. from 90º to 0º. However, this trend was only seen in part 1 and part 2. In part 3, the cylinder at 45º had the maximum cylindricity. Except for cylinder 3, the values of cylindricity were highest in part 3 and lowest in part 1. Hence, it can be said that the cylindricity increases with the wall thickness. As was observed in Figure 37 and Figure 38, the defects in the distorted cylinders on part 1 and part 3 were well captured by the scanner and can be seen in the above figure. As mentioned earlier, cylinder 3 on part 1 was heaviliy distorted and had the maximum cylindricity of all the cylinders.

4.3 Chapter Summary

The results of this work were presented in this chapter. It begins with presenting the values of average surface roughness of different parts. The chapter then advances to the GD & T analysis of the test parts. The results obtained from the visual inspection of the parts were presented and compared with the results obtained using the 3D scanner. The results of dimensional measurements and tolerance analysis were presented. The values obtained using the CMM and the FARO scanner were compared. However, no statistical conclusions were made due to unavailability of multiple part samples.

CHAPTER 5

CONCLUSION AND FUTURE WORK

5.1 Conclusion

In this work, an attempt was made to validate the FARO 3D Scanner for measuring additively manufactured parts. A procedural approach from scanning a part to extracting the details about its geometry, feature tolerances and surface roughness was devised. This study was focused on measurement of surface and geometrical characteristics. Additively manufactured part surfaces are rough and non-uniform. Hence, conventional and industry accepted metrology tools like CMM fail to measure AM parts accurately. The reasons behind this failure were explored. The contact-probe of CMM used in this study has a diameter of 4 mm and it is much too large to find valleys between the peaks which are about 100-200 µm apart. It can be said that in order to capture those valleys, the probe diameter should be much smaller and/or other non-contact techniques could be used to measure AM parts.

It was observed during this study that the 3D scanner collects much more points than a touch probe in lesser time. In case of AM parts, the more points that are collected, the higher the accuracy of the measurements will be. An attempt was made to collect points on the inner cylinders of the hollow cylinders with both the CMM and the scanner. However, neither of the instruments could capture the inner cylinders sufficiently. The scanner fails to reach any intricate surfaces in features like slots and pockets. It was also observed that the FARO scanner generates a little more noise while scanning the AM parts than the machined parts. Further, it was determined that the methodology used and steps performed during scanning are critical

and must be carefully followed. 3D scanning plays a pivotal role and different factors such as part orientation, lighting and scanning coverage must be skilled by the operator.

It was observed that the dimensional measurements obtained using the scanner were within 2% of the measurements obtained by the CMM. However, for tolerances, this percentage was more than 100 and even higher for cylindricity. The scanner was found to capture the defects in the parts sufficiently and it is possible that the scanner might have quantified these defects accurately but there is no way to validate this claim. This is primarily due to the lack of existence of a standard metrology equipment for AM parts.

Therefore, vision based systems like the FARO scanner used in this work can be of great advantage in inspection of AM parts. The accuracy of any system employing an AM process and a vision based inspection tool will depend greatly on the layer thickness used during the build process and the accuracy of the inspection instrument itself. This is because the smaller the layer thickness, the smoother the part surface will be. If the accuracy of the inspection tool is much lesser than the layer thickness, the surface variations would not be captured accurately and hence the measurements will not be accurate.

5.2 Future Work

This work can be used as a stepping stone to explore new opportunities in vision based metrology of AM parts. The approaches described in this work can be used to validate any technology which gives the output in the form of a point cloud. This study can be replicated with more number of samples. Also, more samples with hollow cylinders having different wall thicknesses could be considered. Such an experiment would allow the researcher to perform a Gage R&R study on the data gathered which would possibly help to understand the

performance of the 3D scanner better. Other, more accurate scanners like the ones from Leica (a part of Hexagon Metrology) can be used to generate the point cloud. These experiments can be performed in a controlled atmospheric condition to make sure the lighting does not affect the scan accuracy.

Further, the feature tolerances determined in this study can be used to optimize the overgrowth factor set during the AM process to compensate for shrinkage. If the errors in the features are determined accurately, an overgrowth model can be generated which would essentially predict the amount of machining allowance needed on a particular feature in order to compensate for shrinkage and also to finish-machine it.

This study can prove to be consequential for discovering new in-process inspection options in AM. The flexibility and mobility of the instruments like the FARO scanner could be significantly beneficial in devising an in-process inspection system which will help better monitor the AM process.

REFERENCES

[1] G. Manogharan, “Hybrid Manufacturing: Analysis of Integrating Additive and Subtractive Methods.” North Carolina State University.

[2] P. Bartolo, J.-P. Kruth, J. Silva, G. Levy, A. Malshe, K. Rajurkar, M. Mitsuishi, J. Ciurana, and M. Leu, “Biomedical production of implants by additive electro-chemical and physical processes,” *CIRP Ann. - Manuf. Technol.*, vol. 61, no. 2, pp. 635–655, 2012.

[3] T.-C. Chang, R. Wysk, and H.-P. Wang, *Computer-Aided Manufacturing*, 3rd ed. Pearson.

[4] J. Meadows, *Geometric Dimensioning and Tolerancing- Applications, Analysis & Measurement*. ASME Press.

[5] “ASME Y14.5-2009.” The American Society of Mechanical Engineers.

[6] “Standard Terminology for Additive Manufacturing Technologies F2792-12a.” ASTM Intrnational.

[7] C. K. Chua, K. F. Leong, and Z. H. Liu, “Rapid Tooling in Manufacturing,” in *Handbook of Manufacturing Engineering and Technology*, A. Y. C. Nee, Ed. Springer London, 2015, pp. 2525–2549.

[8] P. Kumar, I. p. s. Ahuja, and R. Singh, “Application of fusion deposition modelling for rapid investment casting – a review,” *Int. J. Mater. Eng. Innov.*, vol. 3, no. 3–4, pp. 204–227, Jan. 2012.

[9] Munish Chhabra and Rupinder Singh, “Rapid casting solutions: a review,” *Rapid Prototyp. J.*, vol. 17, no. 5, pp. 328–350, Aug. 2011.

[10] admin, “Accura® CastPro,” *3D Systems*, 15-Oct-2012. [Online]. Available: http://www.3dsystems.com/materials/accurar-castpro. [Accessed: 01-Jan-2016].

[11] J. W. Halloran, V. Tomeckova, S. Gentry, S. Das, P. Cilino, D. Yuan, R. Guo, A. Rudraraju, P. Shao, T. Wu, T. R. Alabi, W. Baker, D. Legdzina, D. Wolski, W. R. Zimbeck, and D. Long, “Photopolymerization of powder suspensions for shaping ceramics,” *J. Eur. Ceram. Soc.*, vol. 31, no. 14, pp. 2613–2619, Nov. 2011.

[12] admin, “CastForm™ PS,” *3D Systems*, 15-Oct-2012. [Online]. Available: http://www.3dsystems.com/materials/castformtm-ps. [Accessed: 01-Jan-2016].

[13] “EOS Metal Materials for Additive Manufacturing.” [Online]. Available: http://www.eos.info/material-m. [Accessed: 01-Jan-2016].

[14] “S-Print Prototype Printing | ExOne.” [Online]. Available: http://www.exone.com/Systems/Prototyping-Printers/S-Print. [Accessed: 01-Jan-2016].

[15] “industrial 3D printers | voxeljet SYSTEMS.” [Online]. Available: http://www.voxeljet.de/en/systems/. [Accessed: 01-Jan-2016].

[16] “M-Print.” [Online]. Available: http://www.prometal.com/en/materialization/systems/M-Print. [Accessed: 01-Jan-2016].

[17] “What Is Digital Part Materialization?” [Online]. Available: http://www.prometal.com/en/materialization/what-digital-part-materialization. [Accessed: 01-Jan-2016].

[18] “ExOne Introduces Inconel(R) Alloy 625 as Newest Addition to Its 3D Printing Metal Portfolio (NASDAQ:XONE).” [Online]. Available: http://www.investor.exone.com/releasedetail.cfm?releaseid=845102. [Accessed: 18-Jan-2016].

[19] “3D Printing Electronics Laser Additive Manufacturing Systems,” *Optomec Additive Manufacturing*. [Online]. Available: http://www.optomec.com/. [Accessed: 01-Jan-2016].

[20] J. Ruan, L. Tang, T. E. Sparks, R. G. Landers, and F. Liou, “Direct 3D Layer Metal Deposition and Toolpath Generation,” pp. 597–603, Jan. 2008.

[21] K. M. B. Taminger and Robert A. Hafley, “Electron beam freeform fabrication: a rapid metal deposition process,” presented at the 3rd Annual Automotive Composites Conference, Troy, Michigan.

[22] I. Gibson, D. Rosen, and B. Stucker, "*Additive Manufacturing Technologies: 3D Printing, Rapid Prototyping, and Direct Digital Manufacturing"*, 2nd ed., Springer Science + Business Media, Inc.

[23] L. E. Murr, S. M. Gaytan, D. A. Ramirez, E. Martinez, J. Hernandez, K. N. Amato, P. W. Shindo, F. R. Medina, and R. B. Wicker, “Metal Fabrication by Additive Manufacturing

Using Laser and Electron Beam Melting Technologies," *J. Mater. Sci. Technol.*, vol. 28, no. 1, pp. 1–14, Jan. 2012.

[24] D. E. Cooper, M. Stanford, K. A. Kibble, and G. J. Gibbons, "Additive Manufacturing for product improvement at Red Bull Technology," *Mater. Des.*, vol. 41, pp. 226–230, Oct. 2012.

[25] L. Ventola, F. Robotti, M. Dialameh, F. Calignano, D. Manfredi, E. Chiavazzo, and P. Asinari, "Rough surfaces with enhanced heat transfer for electronics cooling by direct metal laser sintering," *Int. J. Heat Mass Transf.*, vol. 75, pp. 58–74, Aug. 2014.

[26] D. T. Pham, S. Dimov, and F. Lacan, "Selective laser sintering: Applications and technological capabilities," *Proc. Inst. Mech. Eng. Part B J. Eng. Manuf.*, vol. 213, no. 5, pp. 435–449, May 1999.

[27] M. W. Khaing, J. Y. H. Fuh, and L. Lu, "Direct metal laser sintering for rapid tooling: processing and characterisation of EOS parts," *J. Mater. Process. Technol.*, vol. 113, no. 1–3, pp. 269–272, Jun. 2001.

[28] M. F. Zaeh and G. Branner, "Investigations on residual stresses and deformations in selective laser melting," *Prod. Eng.*, vol. 4, no. 1, pp. 35–45, Nov. 2009.

[29] Y. Ning, Y. S. Wong, J. Y. H. Fuh, and H. T. Loh, "An approach to minimize build errors in direct metal laser sintering," *IEEE Trans. Autom. Sci. Eng.*, vol. 3, no. 1, pp. 73–80, Jan. 2006.

[30] D. Dimitrov, W. van Wijck, K. Schreve, and N. de Beer, "Investigating the achievable accuracy of three dimensional printing," *Rapid Prototyp. J.*, vol. 12, no. 1, pp. 42–52, Jan. 2006.

[31] T. Ollison and K. Berisso, "Three-dimensional printing build variables that impact cylindricity," *J. Ind. Technol.*, vol. 26, no. 1.

[32] F. M. Megahed, W. H. Woodall, and J. A. Camelio, "A Review and Perspective on Control Charting with Image Data," *J. Qual. Technol.*, vol. 43, no. 2, pp. 83–98, Apr. 2011.

[33] M. J. Milroy, D. J. Weir, D. C. Bradley, and G. W. Vickers, “Reverse engineering employing a 3D laser scanner: A case study,” *Int. J. Adv. Manuf. Technol.*, vol. 12, no. 2, pp. 111–121, Mar. 1996.

[34] Y. Hosni and L. Ferreira, “Laser based system for reverse engineering,” *Comput. Ind. Eng.*, vol. 26, no. 2, pp. 387–394, Apr. 1994.

[35] MATACHE, Gheorghe; DRAGAN, Valeriu; PUSCASU, Cristian; VILAG, Valeriu; PARASCHIV, Alexandru, “A Comparison between 3D Scanning and CMM Dimensional Inspection of Small Size Gas Turbine.” [Online].

[36] T. Várady, R. R. Martin, and J. Cox, “Reverse engineering of geometric models—an introduction,” *Comput.-Aided Des.*, vol. 29, no. 4, pp. 255–268, Apr. 1997.

[37] F. Isgro, F. Odone, and A. Verri, “An open system for 3D data acquisition from multiple sensor,” in *Seventh International Workshop on Computer Architecture for Machine Perception, 2005. CAMP 2005. Proceedings*, 2005, pp. 52–57.

[38] Z. M. Bi and L. Wang, “Advances in 3D data acquisition and processing for industrial applications,” *Robot. Comput.-Integr. Manuf.*, vol. 26, no. 5, pp. 403–413, Oct. 2010.

[39] “FARO 3D Blog – Laser Scanning in a 3D Manufacturing World.” [Online]. Available: http://blog.faro.com/2014/02/laser-scanning-in-a-3d-manufacturing-world/. [Accessed: 18-Jan-2016].

[40] E. Thwaite, “Surface Topography Measurement and Analysis,” *Aust. J. Phys.*, vol. 35, no. 6, pp. 777–784, Jan. 1982.

[41] F. Luk, V. Huynh, and W. North, “Measurement of surface roughness by a machine vision system,” *J. Phys. [E]*, vol. 22, no. 12, p. 977, 1989.

[42] E. Koçer, E. Horozoğlu, and I. Asiltürk, “Noncontact surface roughness measurement using a vision system,” 2015, vol. 9445, pp. 944525–944525–5.

[43] B. Smith, “Making war on defects,” *IEEE Spectr.*, no. 30, Sep. 1993.

[44] T. S. Newman and A. K. Jain, “A Survey of Automated Visual Inspection,” *Comput. Vis. Image Underst.*, vol. 61, no. 2, pp. 231–262, Mar. 1995.

[45] H. Golnabi and A. Asadpour, “Design and application of industrial machine vision systems,” *Robot. Comput.-Integr. Manuf.*, vol. 23, no. 6, pp. 630–637, Dec. 2007.

[46] J. J. Aguilar, F. Torres, and M. A. Lope, “Stereo vision for 3D measurement: accuracy analysis, calibration and industrial applications,” *Measurement*, vol. 18, no. 4, pp. 193–200, Aug. 1996.

[47] J. Molleda, R. Usamentiaga, D. F. García, F. G. Bulnes, A. Espina, B. Dieye, and L. N. Smith, “An improved 3D imaging system for dimensional quality inspection of rolled products in the metal industry,” *Comput. Ind.*, vol. 64, no. 9, pp. 1186–1200, Dec. 2013.

[48] R. J. Valkenburg and A. M. McIvor, “Accurate 3D measurement using a structured light system,” *Image Vis. Comput.*, vol. 16, no. 2, pp. 99–110, Feb. 1998.

[49] J. Xu, N. Xi, C. Zhang, Q. Shi, and J. Gregory, “Real-time 3D shape inspection system of automotive parts based on structured light pattern,” *Opt. Laser Technol.*, vol. 43, no. 1, pp. 1–8, Feb. 2011.

[50] M. Bauza, M. Kirka, R. Bhogaraju, B. Richardson, L. Love, L. Lowe, and R. Dehoff, “Dimensional Accuracy of Large and Complex Ti-6Al-4V Component Made via Electron Beam Melting,” in *ASPE 2015 Spring Topical Meeting*.

[51] M. B. Bauza, S. P. Moylan, R. M. Panas, S. C. Burke, H. E. Martz, J. S. Taylor, P. Alexander, R. H. Knebel, R., and Bhogaraju, M. T. O’Connell, J. D. Smokovitz, “Study of accuracy of parts produced using additive manufacturing,” in *2014 ASPE Spring Topical Meeting: Dimensional Accuracy and Surface Finish in Additive Manufacturing*.

[52] O. Brunke, “phoenix v|tome|x m,” *GE Measurement & Control*, 26-Jan-2015. [Online]. Available: https://www.gemeasurement.com/inspection-ndt/radiography-and-computed-tomography/phoenix-vtomex-m. [Accessed: 17-Jan-2016].

[53] “Computed Tomography | X-ray and CT Inspection | Products | Nikon Metrology.” [Online]. Available: http://www.nikonmetrology.com/en_US/Products/X-ray-and-CT-Inspection/Computed-Tomography. [Accessed: 17-Jan-2016].

[54] T. Vorburger and J. Raja, “Surface Finish Metrology Tutorial.” NIST.gov.

[55] A.S. Iquebal, S. Shrestha, Z. Wang, GP. Manogharan, and S. Bukkapatnam, “Influence of Milling and Non-Traditional Machining on Surface Properties of Ti6Al4V EBM Components,” Proceedings of the 2016 Industrial and Systems Engineering Research Conference.

[56] “FARO Arm User Manual.” Dec-2013.

[57] “Geomgaic Studio User Guide.” .

[58] “PC-DMIS User Manual.” Hexagon Metrology.

APPENDICES

Appendix 1: Other Active Systems

Interferometry: These scanners use a number of stripes or patterns projected simultaneously on the part surface. Two precisely matched pairs of gratings are used to spatially amplitude-modulate the projected light by the grating and the camera grating demodulates the pattern in sight and creates interference fringes whose phases are proportional to the range [38]. These scanners are generally useful when the part under observation has large flat surfaces and small depth variations [38]. Although, these scanners are less accurate than the laser scanners, the incoherent light used eliminates the speckle noise associated with lasers [38].

Time-of-flight or Laser Pulse: These scanners work on the principle that the part surface reflects light back to a receiver which then measures the time for the light to reach the part surface and return back. The range is usually measured as a direct result of the propagation delay of electromagnetic wave. Time-of-flight scanners require very accurate timing sources and they usually have a moderate resolution of a centimeter and occasionally provide an accuracy of a millimeter for longer range applications [38]. These scanners are well suited for environmental modelling and distance measurement at medium to long ranges.

Appendix 2: Surface Roughness MATLAB code

```
X= dlmread ('filename.ext')
[coeff,score,roots] = pca(X);
basis = coeff(:,1:2)
normal = coeff(:,3)
pctExplained = roots' ./ sum(roots)
[n,p] = size(X);
meanX = mean(X,1);
Xfit = repmat(meanX,n,1) + score(:,1:2)*coeff(:,1:2)';
residuals = X - Xfit;
error = abs((X - repmat(meanX,n,1))*normal);
errorsum= sum(error)
Roughness=errorsum/n
```

Appendix 3: Result Tables

1) Dimensional Measurements

Dimension	Features Involved	Part 1				Part 2				Part 3			
		CAD	CMM	FARO	% error	CAD	CMM	FARO	% error	CAD	CMM	FARO	% error
Length	Plane A, Plane C	32.52	32.093	32.1282	-0.10968	32.52	32.202	32.22278	-0.06451	32.52	32.014	32.10973	-0.29901
Height	Plane B, Plane E	32.52	31.492	31.41055	0.258637	32.52	31.252	31.37465	-0.39245	32.52	31.142	31.34748	-0.6598
Width	Plane F, Plane G	19.05	18.72	18.60398	0.619792	19.05	18.749	18.5372	1.12966	19.05	18.731	18.59913	0.704047
Angle AB	Plane A, Plane B	90	89.493	89.229	0.294995	90	89.413	89.38575	0.030477	90	89.337	89.2707	0.074213
Angle BC	Plane B, Plane C	90	89.58	89.5572	0.025452	90	89.846	89.49233	0.393646	90	89.644	89.46155	0.203527
Angle AE	Plane A, Plane E	90	89.427	89.4781	-0.05714	90	89.703	89.52643	0.196844	90	89.683	89.51683	0.185292
Angle BD	Plane B, Plane D	45	44.494	44.78413	-0.65205	45	44.704	44.8075	-0.23152	45	44.258	44.85433	-1.34738
Angle Cyl.1	Cylinder 1	90	89.528	89.76	-0.25914	90	89.89	89.82953	0.067277	90	89.306	89.5131	-0.2319
Angle Cyl.2	Cylinder 2	45	44.547	44.8892	-0.76818	45	44.82	44.96848	-0.33127	45	45.489	44.98615	1.105432
Angle Cyl.3	Cylinder 3	0	0.447	0.51555	-15.3356	0	0.335	0.323675	3.380597	0	0.236	0.1298	45
Diameter Cyl.1	Cylinder 1	11.43	11.2675	11.06883	1.763257	10.16	10.05125	9.863775	1.865191	12.7	12.36475	12.23415	1.056228
Diameter Cyl.2	Cylinder 2	11.43	11.17033	10.5918	5.179195	10.16	10.03525	10.10505	-0.69555	12.7	12.238	11.73768	4.088291
Diameter Cyl.3	Cylinder 3	11.43	10.96325	10.9937	-0.27775	10.16	10.056	10.03513	0.207588	12.7	12.41775	12.28033	1.106682

2) Tolerances

Tolerance	Features Involved	Part 1			Part 2			Part 3		
		CMM	FARO	% error	CMM	FARO	% error	CMM	FARO	% error
Flatness	Plane A	0.282	0.44975	-59.4858	0.294	0.36825	-25.2551	0.24	0.36505	-52.1042
Flatness	Plane B	0.227	0.489175	-115.496	0.226	0.5888	-160.531	0.137	0.427725	-212.208
Cylindricity	Cylinder 1	0.073	0.328125	-349.486	0.102	0.42835	-319.951	0.154	0.4796	-211.429
Cylindricity	Cylinder 2	0.407	0.6058	-48.8452	0.133	0.504725	-279.492	0.207	0.6517	-214.831
Cylindricity	Cylinder 3	0.906	1.014125	-11.9343	0.112	0.65835	-487.813	0.169	0.503575	-197.973

The above tables show the results obtained from this study. It should be noted that the percentage error in these tables corresponds to the percentage error between the CMM and FARO measurements.